

Fusion or Confusion? Multimodal Complexity Is Not All You Need

Tillmann Rheude¹ Roland Eils^{1 2 3} Benjamin Wild¹

Abstract

Deep learning architectures for multimodal learning have increased in complexity, driven by the assumption that multimodal-specific methods improve performance. We challenge this assumption through a large-scale empirical study reimplementing 19 high-impact methods under standardized conditions. We evaluate them across nine diverse datasets with up to 23 modalities, and test their generalizability to new tasks beyond their original scope, including settings with missing modalities. We propose a **Simple Baseline for Multimodal Learning** (SimBaMM), a late-fusion Transformer architecture, and demonstrate that under standardized experimental conditions with rigorous hyperparameter tuning of all methods, more complex architectures do not reliably outperform SimBaMM. Statistical analyses show that complex methods perform on par with SimBaMM and often fail to consistently outperform well-tuned unimodal baselines, especially in small-data settings. To support our findings, we include a case study highlighting common methodological shortcomings in the literature followed by a pragmatic reliability checklist to promote comparable, robust, and trustworthy future evaluations. In summary, we argue for a shift in focus: away from the pursuit of architectural novelty and toward methodological rigor.⁴

1. Introduction

The pursuit of state-of-the-art (SoTA) performance in multimodal learning has led to increasingly complex architectures. The field is engaged in an architectural arms race, driven by the implicit assumption that novel fusion mech-

¹Berlin Institute of Health, Charité - Universitätsmedizin Berlin

²Intelligent Medicine Institute, Fudan University ³Department of Mathematics and Computer Science, Freie Universität Berlin. Correspondence to: Benjamin Wild <benjamin.wild@bih-charite.de>, Roland Eils <roland.eils@bih-charite.de>, Tillmann Rheude <tillmann.rheude@bih-charite.de>.

Preprint. January 15, 2026.

⁴The code repository is available on [GitHub](#).

anisms, gradient-based regularization, and deeper, more sophisticated networks are the primary drivers of progress. This has resulted in a landscape in which models are often celebrated for their structural novelty, with performance gains on specific benchmarks presented as evidence of their superiority. However, such gains are difficult to interpret when evaluation protocols differ across papers and when key experimental factors, *e.g.*, hyperparameter tuning, weight initialization, and missing-modality simulation, are not consistently controlled. In this paper, we challenge this prevailing narrative that architectural novelty is the primary driver of performance in multimodal learning. We argue that methodological rigor in model selection and evaluation can explain a substantial portion of reported improvements. Accordingly, we hypothesize that performance gains often attributed to complex design choices may not reliably persist under standardized experimental conditions. To substantiate this claim, we perform a large-scale empirical study evaluating 19 multimodal architectures across nine datasets with up to 488 131 samples and up to 23 modalities. Our goal is to disentangle the contributions of architectural complexity from those of experimental practice. Our findings reveal that increased architectural complexity does not yield consistent gains over a simple late-fusion baseline when all methods are tuned and evaluated under the same rigorous protocol. Our contributions are summarized as follows:

- **A large-scale benchmark of multimodal architectures under a unified protocol** We re-implement and evaluate 19 multimodal methods across nine datasets, enabling controlled comparisons and assessing performance transfers beyond the original evaluation settings.
- **A Simple Baseline for Multimodal Learning (SimBaMM)** We introduce SimBaMM, a late-fusion Transformer baseline that handles missing modalities through masking (Figure 1). SimBaMM matches or exceeds the performance of more complex models under rigorous tuning and standardized evaluation.
- **A case study revealing how experimental confounders inflate reported performance** We demonstrate weaknesses in the literature, such as information leakage during validation and inadequate hyperparameter tuning, by including a case study of a recent multimodal learning method.

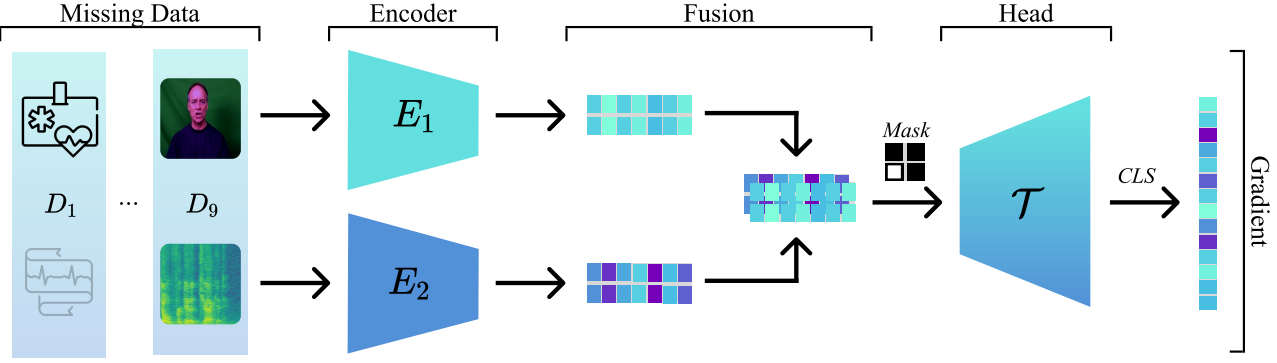


Figure 1. Taxonomy of multimodal learning methods exemplified by two modalities. A late-fusion baseline (SimBaMM) processes a multimodal dataset D with up to M modalities through encoders E_m , combines them via fusion, and produces predictions through a classification head. Categorized into five groups, we evaluate 19 SoTA methods across nine datasets based on their architectural innovations on top of SimBaMM: **Missing Data** handling for incomplete modalities, *e.g.*, a missing ECG, **Encoder**-level modifications, **Fusion** mechanisms for combining representations, **Head**-based cross-modal architectures, and **Gradient**-based optimization techniques. Our large-scale empirical study reveals that none of these complex extensions reliably outperforms SimBaMM, suggesting that reported performance gains are often attributable to experimental confounders rather than methodological novelty.

2. Related Work

Multimodal Learning Multimodal learning addresses the use of multiple modalities to perform prediction tasks. We focus on architectural contributions to multimodal learning rather than multimodality-specific applications. Architectures in multimodal deep learning can be divided into groups (Figure 1) spanning missing-data handling (Wang et al., 2023b; Nezakati et al., 2024; Wang et al., 2023a), encoder developments (Ghahremani & Wachinger, 2023; Jiang et al., 2025), fusion mechanisms (Nagrani et al., 2021; Liu et al., 2018; Cao et al., 2024; Li et al., 2024; Wu et al., 2025), head models (Tsai et al., 2019), and gradient regulation methods (Peng et al., 2022; Wei et al., 2025a;b; Wei & Hu, 2024; Wu et al., 2022; Wang et al., 2020). There is also work on meta-learning (Ma et al., 2021) and similar extensions such as pre-training or distillation (Li et al., 2021) to multimodal learning, which are excluded in our work. Recent work conducted a large-scale study of scaling laws for native multimodal models, comparing primarily early- and late-fusion designs (Shukor et al., 2025). This line of work both supports and contextualizes our approach: their scaling results motivate our use of a simple late-fusion transformer, while our study targets a different gap by benchmarking a broad set of contemporary multimodal methods across diverse datasets with statistically rigorous evaluation and model selection. Furthermore, our work is situated within the context of large-scale multimodal benchmarking, with MultiBench (Liang et al., 2021) representing the most closely related effort. However, we extend and differentiate our work from this foundation and the aforementioned work in several ways. First, we evaluate generalizability on a curated set of large-scale, contemporary real-world datasets. Second, we assess cross-domain performance directly (rather than splitting in- vs. out-of-domain) to attribute gains to method-

ological contributions and test their transferability (Lipton & Steinhardt, 2019). Third, we standardize key implementation details such as weight initializations. Finally, we introduce SimBaMM that addresses the reliability aspect of multimodal learning that was previously underexplored in the literature. In contrast to a general benchmark, our work is a cohesive comparative study that establishes a strong, up-to-date baseline for the field. In summary, we do not seek to advance multimodal architectures but to test whether recent methodological advances withstand rigorous evaluation.

Multimodal Learning with Missing Modalities Prior work on robustly handling missing modalities is broadly classified into two categories: strategy design (which includes architecture-focused designs and model combinations) and data processing (which involves representation learning and modality imputation) (Wu et al., 2024). If missing modalities are not imputed directly at the data level, prior knowledge about missing modalities is used to engineer modules for handling missing modalities. This can, *e.g.*, be done with latent space reconstructions (Wang et al., 2023b) or projections (Nezakati et al., 2024), and distribution alignments (Wang et al., 2023a). On the other hand, Transformers (Vaswani et al., 2017) are able to handle missing modalities since they can handle arbitrary sequence lengths. Even if prior work reports performance drops with missing modalities and finds that standard Transformers degrade in this setting (Ma et al., 2022), balanced training with missing modalities can be sufficient for downstream performance (Memmel et al., 2023). Yet, a large-scale, domain-independent study of such a Simple Baseline (SimBa) is still lacking.

Reproducibility of Machine Learning Methods According to prior work, machine learning suffers from a repro-

ducibility crisis (Kapoor & Narayanan, 2023; Semmelrock et al., 2025). For example, there is prior work focusing on reproducibility in healthcare (McDermott, 2025) and guidelines for reproducibility in life sciences (Heil et al., 2021). More generally, venues for high-impact machine learning publications are aware of this crisis, *i.e.*, by offering solutions such as reproducibility challenges and reports (Pineau et al., 2021). Nevertheless, we consider not only reproducibility, but also the problem of practically unsound comparisons, *e.g.*, comparing architectures without adequate hyperparameter optimization.

Simple Baselines (SimBas) A variety of SimBas exists for different tasks and settings. For example, for computer vision tasks, there is related work regarding SimBas for video restoration (Li et al., 2023a), tracking (Lin et al., 2022), image classification (Chan et al., 2015; Liu et al., 2022b), video text spotting (He et al., 2024), hand mesh reconstruction (Zhou et al., 2024), graph generation (Shi et al., 2021), video matting (Li et al., 2023b), spoken-to-sign-language translation (Zuo et al., 2024), and point cloud classification (Goyal et al., 2021). More general approaches tackle, *e.g.*, active learning (Kirsch et al., 2023), Bayesian uncertainty (Maddox et al., 2019), transfer learning (Chen et al., 2022), continual learning (Buzzega et al., 2020; Prabhu et al., 2020; Press et al., 2023; Zhang et al., 2022), the traveling salesman problem (Xia et al., 2024), time series (Chen et al., 2025), knowledge tracing (Liu et al., 2023), and instruction fine-tuning (Zhao et al., 2024). In the context of multimodal learning, there is prior work related to multimodal image segmentation (Bastico et al., 2023), multimodal medical reasoning (Huang et al., 2025), multimodal embeddings (Liang et al., 2019), multimodal representation learning (Manolache et al., 2024), multimodal Vision-Language Models (VLMs) (Xu et al., 2024), multimodal learning with Mixture of Experts (MoE) models (Li et al., 2025), and multimodal domain generalization (Dong et al., 2023). Additionally, prior work hints that there is no benefit of multimodal extensions, *e.g.*, different fusion models (Song et al., 2024), more complex methods (Caranzano et al., 2025), or pre-training in genomics (Vishniakov et al., 2024). However, all these SimBas are usually related to a specific domain or limited to small ablation studies, and do not investigate generalization across multiple domains. In summary, such an analysis for multimodal learning across all architectural components is currently missing.

3. Method

We consider a dataset $D = \{(\{x_{i,m}\}_{m \in \mathcal{M}_i}, y_i)\}_{i=1}^N$ consisting of N samples. Each sample i is composed of inputs from a (sub)set of M possible modalities and a corresponding target label y_i . We denote the set of available modality indices as $\mathcal{M}_i \subseteq \{1, \dots, M\}$. For an available modality

$m \in \mathcal{M}_i$, the input is $x_{i,m}$.

3.1. Simple Baseline for Multimodal Learning (SimBaMM)

The SimBaMM architecture processes each sample through a multi-stage late-fusion pipeline (Figure 1).

Encoders For each available modality $m \in \mathcal{M}_i$, the input $x_{i,m}$ is passed through a modality-specific encoder E_m to obtain an embedding $e_{i,m} = E_m(x_{i,m})$. To harmonize representations across modalities, each embedding $e_{i,m}$ is projected into a shared hidden space of dimension d using a modality-specific linear layer P_m : $\hat{e}_{i,m} = P_m(e_{i,m}) \in \mathbb{R}^d$.

Fusion We form an input sequence S_i from the projected embeddings. To balance performance and fine-grained modeling, we study two variants: (i) **SimBaMM**, which uses a configurable number of tokens per modality (determined by the encoder output and a pooling/tokenization choice), and (ii) **SimBaMM^{CLS}**, which represents each modality by a single token, *e.g.*, a `[CLS]` embedding, yielding a fixed multimodal sequence length of M with padding.

Head The head module is a Transformer \mathcal{T} operating over S_i . To handle missing modalities, we construct an attention mask $M_{\text{attn}}(\mathcal{M}_i)$ such that attention is only computed among tokens originating from available modalities. This enables a controlled comparison between mask-only handling and the additional mechanisms used in prior work. The fused representation is $H_i = \mathcal{T}(S_i, M_{\text{attn}}(\mathcal{M}_i))$. Afterwards, a projection $g(\cdot)$ maps the fused representation H_i to a task-specific output $\hat{y}_i = g(H_i)$. We optimize a task loss $\mathcal{L}(y_i, \hat{y}_i)$, *i.e.*, (binary) cross-entropy.

3.2. Comparison Taxonomy, Method Selection & (Re-)Implementations

We group multimodal methods by the type of innovation they introduce beyond late fusion. Figure 1 summarizes SimBaMM and the resulting comparison groups used throughout the experiments. We benchmark SimBaMM against a representative set of recent and influential multimodal methods to test whether architectural and objective-level innovations provide consistent gains under a rigorous evaluation protocol. Methods were selected to cover the comparison taxonomy in Figure 1 based on: (a) recency (primarily methods from the last few years), (b) publication in top-tier peer-reviewed machine learning venues, and (c) explicit architectural or objective-based modifications beyond a standard late-fusion baseline. We prioritize methods with sufficiently detailed specifications and/or official reference implementations to enable faithful re-implementations. Full details of all 19 compared multimodal architectures and re-implementations are provided in Section A. All models are

Table 1. Overview of benchmark datasets and the respective encoders used in our evaluation. Further details in Section D.

Dataset	# Samples	# Modalities	Modalities	Raw Input	Encoders
MIMIC HAIM	45,050	2	Laboratory, X-ray	✓	MLP, ViT
MIMIC Symile	10,345	3	Laboratory, X-ray, ECG	✓	MLP, ViT, Transformer
INSPECT	22,449	2	CT, EHR	✗	MLPs
UKB	488,131	23	e.g., Metabolomics, EHR, PRS, Proteomics, Blood Biochemistry	✓ ✗	MLPs
CMU-MOSI	2,199	3	Video, Audio, Language	✗	2× Transformer, BERT
CMU-MOSEI	22,856	3	Video, Audio, Language	✗	2× Transformer, BERT
CH-SIMS	2,281	3	Video, Audio, Language	✓	ViViT, Wav2Vec2, BERT
CH-SIMS 2	4,403	3	Video, Audio, Language	✓	ViViT, Wav2Vec2, BERT
Crema-D	7,442	2	Video, Audio	✓	2× ResNet

implemented in a shared codebase using PyTorch Lightning (Falcon & The PyTorch Lightning team, 2019) to ensure consistent training, logging, and evaluation. Encoders are dataset-specific but held fixed across all methods (Table 1).

Generalization to heterogeneous benchmarks Reference implementations typically assume a fixed number of modalities, specific modality types, and a single downstream task. We adapt all methods to (i) an arbitrary number of modalities, (ii) heterogeneous modality types, and (iii) different tasks and loss functions while preserving the original method’s defining components. If a method introduces auxiliary losses, we include them; if auxiliary-loss weighting is not specified, we introduce scalar weights and tune them under the same protocol as other hyperparameters.

Token propagation and computational comparability Unless a method architecturally requires full token sequences, *e.g.*, cross-attention between modality token sequences, we propagate a single modality token, *e.g.*, a [CLS] representation, from each encoder for efficiency and to keep bandwidth comparable across methods.

Optimization and initialization To reduce the degrees of freedom and improve comparability, we adopt a common optimizer choice whenever compatible with the method. By default, we use the ScheduleFree (Defazio et al., 2024) variant of AdamW and SGD only when required by the method. Weight initializations are standardized across methods.

3.3. Experimental Protocols

Missing-modality protocol We simulate missing modalities at the dataset-split level (rather than per batch) to ensure consistent and reproducible training conditions across epochs (Rheude et al., 2025). Concretely, we pre-generate a binary missingness mask for all samples in a split. Missing rates are defined per number of missing modalities: for a trimodal dataset, a rate of 15% means 15% of samples miss exactly one and another 15% miss exactly two modalities.

Hyperparameter tuning protocol We first conduct a Bayesian hyperparameter search for SimBaMM over a fixed set of parameters and an extensive search space to determine robust base configurations, *e.g.*, encoder/head dimensions. These base settings are then used as a starting point for tuning the remaining methods, focusing on method-specific components and optimizer parameters under a controlled tuning budget (Section G). As a counterexample, we tune the full hyperparameter space of one method independently of SimBaMM and find that this exhaustive per-method tuning does not materially change the results or conclusions (Section E). Details in Section A.

Bayesian statistical comparison To rigorously compare methods across datasets, we employ Bayesian hierarchical analysis following Corani et al. (2017) and Benavoli et al. (2017). This allows us to account for correlations between cross-validation folds and estimate the posterior probability of three outcomes: (1) method *A* outperforms *B* by > 1%, (2) method *B* outperforms *A* by > 1%, or (3) they are practically equivalent (difference within a $\pm 1\%$ Region of Practical Equivalence (ROPE)). Details in Section F.

4. Experiments

4.1. Multimodal Datasets

We evaluate all methods on nine real-world multimodal datasets (Table 1) ranging from 2199 to 488 131 samples, 2 to 23 modalities, and covering tasks from healthcare to emotion recognition: MIMIC Symile (Saporta et al., 2024), MIMIC Haim (Soenksen et al., 2022a;b), INSPECT (Huang et al., 2023), UK Biobank (UKB) (Sudlow et al., 2015), MOSI (Zadeh et al., 2016), MOSEI (Zadeh et al., 2018), CH-SIMS (Yu et al., 2020), CH-SIMS v2 (Liu et al., 2022a), and Crema-D (Cao et al., 2014). These datasets differ in both their input modalities and data representations, while remaining non-synthetic and representative of real-world tasks. For the UKB, missing modalities are an inherent characteristic. Therefore, we implemented zero imputation

Table 2. Performance in terms of AUROC across various healthcare datasets. Details including full unimodal results in Section D. No method is highlighted because performance differences fall within the reported mean \pm standard deviations (SDs), summarized in Table 4.

Method	HAIM \uparrow	Symile \uparrow	INSPECT \uparrow	UKB \uparrow
Best Unimodal	$0.7042 \pm .020$	$0.6453 \pm .030$	$0.6568 \pm .003$	$0.7560 \pm .010$
<i>Missing Data-Based</i>				
IMDer (Wang et al., 2023b)	$0.6900 \pm .018$	$0.6266 \pm .016$	$0.6385 \pm .007$	$0.7969 \pm .003$
MMP (Nezakati et al., 2024)	$0.6611 \pm .016$	$0.5824 \pm .054$	$0.6289 \pm .018$	$0.7984 \pm .004$
ShaSpec (Wang et al., 2023a)	$0.6863 \pm .019$	$0.5823 \pm .052$	$0.6348 \pm .006$	$0.7968 \pm .007$
SimBaMM ^{CLS}	$0.6558 \pm .031$	$0.5925 \pm .045$	$0.6378 \pm .008$	$0.7957 \pm .008$
SimBaMM	$0.6600 \pm .024$	$0.6262 \pm .023$	n/a	n/a
<i>Encoder-Based</i>				
RegBN (Ghahremani & Wachinger, 2023)	$0.6912 \pm .054$	$0.6412 \pm .018$	$0.6379 \pm .002$	$0.7919 \pm .001$
AUG (Jiang et al., 2025)	$0.7103 \pm .027$	$0.6101 \pm .035$	$0.6513 \pm .016$	$0.7361 \pm .136$
<i>Fusion-Based</i>				
MBT (Nagrani et al., 2021)	$0.6804 \pm .029$	$0.6331 \pm .023$	$0.6391 \pm .003$	$0.7456 \pm .106$
LMF (Liu et al., 2018)	$0.7181 \pm .037$	$0.6146 \pm .023$	$0.6454 \pm .003$	$0.4999 \pm .000$
PDF (Cao et al., 2024)	$0.6880 \pm .025$	$0.5922 \pm .020$	$0.6419 \pm .003$	$0.7825 \pm .014$
Coupled Mamba (Li et al., 2024)	$0.6631 \pm .040$	$0.6603 \pm .027$	$0.6580 \pm .004$	$0.7974 \pm .003$
OMIB (Wu et al., 2025)	$0.7040 \pm .019$	$0.5922 \pm .038$	$0.6272 \pm .008$	$0.6262 \pm .070$
<i>Head-Based</i>				
MuLT (Tsai et al., 2019)	$0.6872 \pm .030$	$0.6374 \pm .014$	$0.6510 \pm .004$	OOM
<i>Gradient-Based</i>				
OGM (Peng et al., 2022)	$0.7172 \pm .014$	$0.6138 \pm .011$	$0.6431 \pm .005$	$0.7982 \pm .013$
OGM ^{GE} (Peng et al., 2022)	$0.7069 \pm .030$	$0.6152 \pm .034$	$0.6426 \pm .002$	$0.7982 \pm .008$
DGL (Wei et al., 2025a)	$0.6143 \pm .066$	$0.6032 \pm .017$	$0.6276 \pm .043$	$0.5803 \pm .053$
ARL (Wei et al., 2025b)	$0.7000 \pm .024$	$0.6393 \pm .032$	$0.6514 \pm .002$	$0.7986 \pm .003$
MMPareto (Wei & Hu, 2024)	$0.7021 \pm .029$	$0.6319 \pm .038$	$0.6559 \pm .005$	$0.8054 \pm .009$
BMML (Wu et al., 2022)	$0.7072 \pm .034$	$0.6419 \pm .020$	$0.6233 \pm .003$	$0.7940 \pm .003$
G-Blend Online (Wang et al., 2020)	$0.7123 \pm .028$	$0.6179 \pm .084$	$0.6538 \pm .005$	$0.8036 \pm .014$
G-Blend Offline (Wang et al., 2020)	$0.7148 \pm .032$	$0.6050 \pm .067$	$0.6284 \pm .018$	$0.7795 \pm .033$
SimBaMM ^{CLS}	$0.6985 \pm .025$	$0.6318 \pm .015$	$0.6556 \pm .006$	$0.7957 \pm .008$
SimBaMM	$0.6871 \pm .029$	$0.6429 \pm .036$	n/a	n/a

for this dataset except for the missing data-based methods. Input modalities are z-score normalized for all datasets. Depending on the modality, we use a Multi-Layer Perceptron (MLP), Vision Transformer (ViT) (Dosovitskiy et al., 2021), Transformer (Vaswani et al., 2017), BERT (Devlin et al., 2019), Wav2Vec2 (Baevski et al., 2020), ViViT (Arnab et al., 2021), or ResNet (He et al., 2016) as encoders. We report mean and SD using subject-wise five-fold cross-validation. This eliminates subject overlap between folds, addressing both a frequent methodological weakness in the field (see Section 4.4) and the ability to generalize to new samples. Details in Section D.

4.2. Downstream Task Analysis

We provide a comprehensive empirical comparison of SimBaMM against the 19 re-implemented SoTA methods, including unimodal performance, for healthcare and emotion recognition (Tables 2 and 3). Additionally, we provide a detailed analysis of different missing rates (Figure 2). For datasets without a sequence dimension, SimBaMM reduces

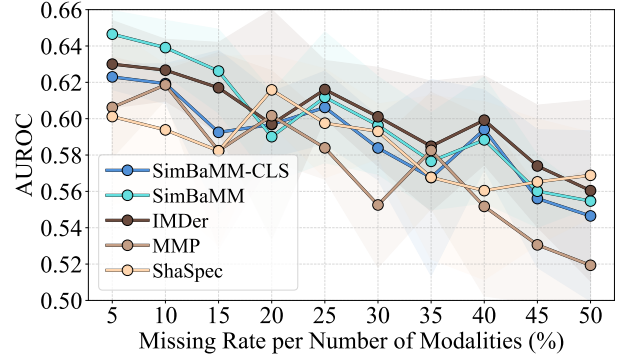


Figure 2. Missing-modality analysis on MIMIC Symile: methods perform similarly across missing rates, with overlapping SDs.

to SimBaMM^{CLS}, resulting in n/a for the other SimBaMM variant. Use cases with many modalities ($M \gg 2$) are common in healthcare, shown with the UKB (Table 2). However, MuLT and LMF become unstable in this setting. MuLT scales quadratically, requiring $M(M - 1)$ cross-modal transform-

Table 3. Performance for emotion recognition in terms of Acc_7 (MOSI/MOSEI), Acc_5 (CH-SIMS/CH-SIMS2) and Acc_6 (Crema-D). No method is highlighted because performance differences fall within the reported mean \pm SDs, summarized in Table 4.

Method	MOSI \uparrow	MOSEI \uparrow	CH-SIMS \uparrow	CH-SIMS 2 \uparrow	Crema-D \uparrow
<i>Unimodal</i>					
Language	$0.4084 \pm .024$	$0.5144 \pm .006$	$0.5458 \pm .022$	$0.4280 \pm .014$	n/a
Vision	$0.2556 \pm .038$	$0.4285 \pm .007$	$0.3593 \pm .014$	$0.2497 \pm .010$	$0.3192 \pm .027$
Audio	$0.2401 \pm .011$	$0.4197 \pm .005$	$0.4298 \pm .021$	$0.2686 \pm .031$	$0.6081 \pm .032$
<i>Missing Data-Based</i>					
IMDer (Wang et al., 2023b)	$0.2810 \pm .058$	$0.4273 \pm .039$	$0.4541 \pm .079$	$0.3951 \pm .022$	$0.6840 \pm .032$
MMP (Nezakati et al., 2024)	$0.2451 \pm .046$	$0.2760 \pm .117$	$0.4201 \pm .127$	$0.3589 \pm .024$	$0.6552 \pm .025$
ShaSpec (Wang et al., 2023a)	$0.28921 \pm .031$	$0.3489 \pm .111$	$0.4806 \pm .026$	$0.4222 \pm .015$	$0.6051 \pm .034$
SimBaMM ^{CLS}	$0.2683 \pm .057$	$0.3769 \pm .083$	$0.4716 \pm .062$	$0.4059 \pm .017$	$0.6380 \pm .039$
SimBaMM	$0.3028 \pm .060$	$0.4169 \pm .076$	$0.5122 \pm .047$	$0.4090 \pm .012$	n/a
<i>Encoder-Based</i>					
RegBN (Ghahremani & Wachinger, 2023)	$0.2115 \pm .096$	$0.3894 \pm .069$	$0.4704 \pm .057$	$0.4135 \pm .034$	$0.6340 \pm .026$
AUG (Jiang et al., 2025)	$0.2756 \pm .067$	$0.4395 \pm .022$	$0.4797 \pm .050$	$0.3715 \pm .025$	$0.6105 \pm .029$
<i>Fusion-Based</i>					
MBT (Nagrani et al., 2021)	$0.3124 \pm .053$	$0.4434 \pm .030$	$0.5113 \pm .058$	$0.4367 \pm .016$	$0.6525 \pm .018$
LMF (Liu et al., 2018)	$0.2842 \pm .042$	$0.3704 \pm .087$	$0.5020 \pm .051$	$0.4074 \pm .021$	$0.6363 \pm .013$
PDF (Cao et al., 2024)	$0.3315 \pm .048$	$0.4649 \pm .020$	$0.5109 \pm .042$	$0.4006 \pm .015$	$0.5976 \pm .028$
Coupled Mamba (Li et al., 2024)	$0.3147 \pm .037$	$0.5188 \pm .005$	$0.5209 \pm .041$	$0.4448 \pm .010$	$0.6792 \pm .040$
OMIB (Wu et al., 2025)	$0.3211 \pm .015$	$0.4795 \pm .011$	$0.4535 \pm .075$	$0.4105 \pm .029$	$0.6690 \pm .046$
<i>Head-Based</i>					
MuLT (Tsai et al., 2019)	$0.3584 \pm .031$	$0.5147 \pm .006$	$0.4979 \pm .102$	$0.3993 \pm .100$	$0.6102 \pm .037$
<i>Gradient-Based</i>					
OGM (Peng et al., 2022)	$0.2883 \pm .063$	$0.3060 \pm .176$	$0.4766 \pm .052$	$0.3927 \pm .019$	$0.6185 \pm .043$
OGM ^{GE} (Peng et al., 2022)	$0.3147 \pm .026$	$0.4274 \pm .054$	$0.5617 \pm .031$	$0.3688 \pm .024$	$0.6281 \pm .031$
DGL (Wei et al., 2025a)	$0.3533 \pm .046$	$0.3253 \pm .143$	$0.3948 \pm .053$	$0.2471 \pm .039$	$0.6717 \pm .033$
ARL (Wei et al., 2025b)	$0.2574 \pm .073$	$0.2838 \pm .132$	$0.5570 \pm .013$	$0.4579 \pm .008$	$0.6318 \pm .032$
MMPareto (Wei & Hu, 2024)	$0.3488 \pm .067$	$0.4209 \pm .055$	$0.5373 \pm .035$	$0.4354 \pm .030$	$0.4398 \pm .046$
BMML (Wu et al., 2022)	$0.2287 \pm .056$	$0.4307 \pm .100$	$0.5514 \pm .035$	$0.4255 \pm .041$	$0.6535 \pm .067$
G-Blend Online (Wang et al., 2020)	$0.2519 \pm .064$	$0.4128 \pm .066$	$0.5139 \pm .028$	$0.4503 \pm .010$	$0.5566 \pm .069$
G-Blend Offline (Wang et al., 2020)	$0.2383 \pm .086$	$0.4290 \pm .066$	$0.5311 \pm .017$	$0.4101 \pm .023$	$0.6241 \pm .023$
SimBaMM ^{CLS}	$0.3229 \pm .054$	$0.4936 \pm .015$	$0.5086 \pm .042$	$0.4351 \pm .014$	$0.6723 \pm .031$
SimBaMM	$0.3056 \pm .080$	$0.3950 \pm .101$	$0.5276 \pm .059$	$0.4326 \pm .028$	n/a

ers (506 for $M=23$), which is memory-prohibitive. LMF’s multiplicative fusion leads to vanishing gradients and activation collapse (AUROC \approx random), suggesting tensor-product fusion is ill-suited for $M \gg 2$. For a summarizing comparison of all methods (Section 3.3 and Details in Section F), we aim to answer two critical questions:

Does multimodal complexity yield performance gains? Our analysis suggests limited evidence for practically meaningful performance gains from multimodal complexity. No complex method achieves a high probability of outperforming SimBaMM (Table 4). The single highest probability of a complex method winning is $\approx 30\%$ (C-Mamba). Conversely, for methods like AUG, DGL, and OMIB, SimBaMM^{CLS} is almost certainly superior ($P(\text{Base} > \text{Method}) \geq 95\%$). For the strongest competitors (C-Mamba, MMPareto), the data supports practical equivalence ($P_{\text{ROPE}} \approx 70\%$), indicating limited evidence for a consistent $\geq 1\%$ improvement over the baseline.

Do multimodal methods improve upon unimodal baselines? Given our empirical results, multimodal methods do not reliably improve upon unimodal baselines (Table 8). While C-Mamba ($\approx 72\%$) and ARL ($\approx 67\%$) likely outperform the best unimodal baseline, many complex architectures, *e.g.*, DGL, OMIB, LMF, and PDF are likely *worse* than simply using the best single modality ($P(\text{Unimodal} > \text{Method}) > 80\%$). SimBaMM^{CLS} ($\approx 53\%$) rivals the top complex methods in its ability to outperform unimodal baselines, suggesting that multimodal architectural complexity does not reliably yield meaningful performance improvements for the multimodal datasets in our study.

4.3. Efficiency Analysis

We analyze the selected methods in terms of Floating Point Operations (FLOPS), number of parameters, and runtime per epoch to demonstrate that many complex models incur high computational costs without yielding improvements in

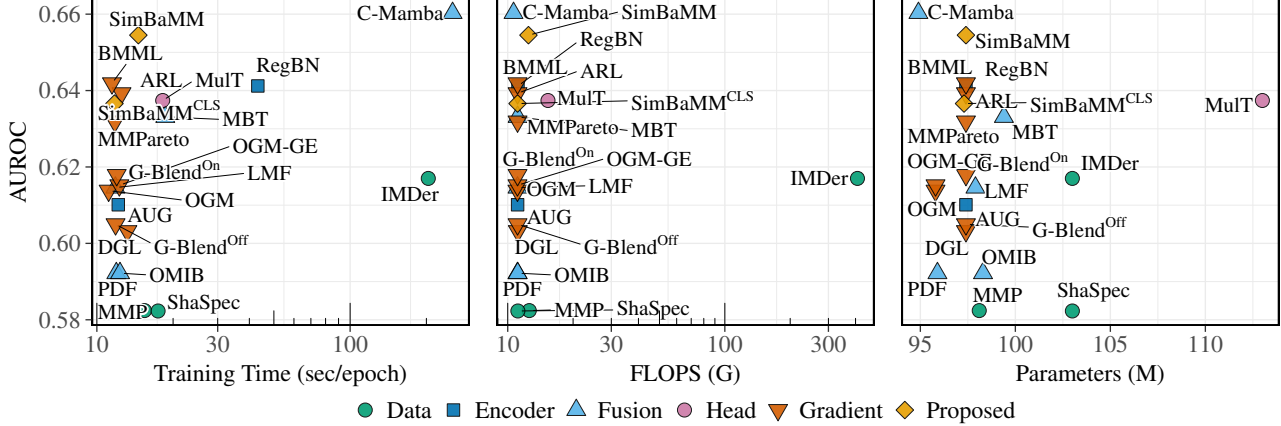


Figure 3. Efficiency analysis for training time (left), FLOPS (middle), and parameters (right) on the MIMIC Symile dataset. Regardless of the metric, SimBaMM and SimBaMM^{CLS} perform consistently while others, e.g., Coupled Mamba and IMDer are metric-dependent.

Table 4. Comparison with SimBaMM^{CLS} (base in this table). No method achieves a high probability of meaningfully outperforming SimBaMM^{CLS}. Details in Section F.

Method	P(base >other)	P(\approx >other)	P(other >base)	$\mathbb{E}[\delta_0]$	95% CI
Best Unimodal	0.53	0.06	0.41	0.002	[-0.031, 0.031]
C-Mamba	0.03	0.67	0.30	-0.006	[-0.021, 0.006]
MMPareto	0.13	0.67	0.19	-0.002	[-0.019, 0.022]
ARL	0.30	0.47	0.23	0.002	[-0.019, 0.028]
GBlend-On	0.36	0.48	0.16	0.005	[-0.018, 0.045]
BMML	0.75	0.05	0.19	0.013	[-0.021, 0.051]
OGM ^{GE}	0.77	0.16	0.06	0.015	[-0.009, 0.042]
MuLT	0.33	0.41	0.26	0.002	[-0.023, 0.031]
SimBaMM	0.52	0.23	0.25	0.007	[-0.038, 0.056]
MBT	0.68	0.29	0.03	0.012	[-0.004, 0.028]
GBlend-Off	0.90	0.06	0.04	0.021	[-0.005, 0.048]
LMF	0.89	0.01	0.10	0.049	[-0.028, 0.142]
OMIB	0.95	0.04	0.01	0.022	[0.003, 0.043]
OGM	0.85	0.12	0.03	0.017	[-0.003, 0.040]
PDF	0.94	0.05	0.01	0.020	[0.005, 0.037]
AUG	0.97	0.01	0.02	0.032	[-0.000, 0.066]
RegBN	0.75	0.22	0.03	0.014	[-0.004, 0.039]
DGL	0.98	0.00	0.02	0.078	[0.006, 0.158]

downstream performance (Figure 3). For instance, IMDer requires 203s of runtime and 408 GFLOPS because of diffusion steps, yet only achieves an AUROC of 0.6170. Similarly, MuLT, which has the largest number of parameters (113M), results in a lower AUROC of 0.6374 compared to more parameter-efficient models. While C-Mamba reaches the highest AUROC (0.6603), it comes at the cost of a prohibitive runtime of 253s. In contrast, SimBaMM demonstrates a balance of efficiency and effectiveness. It achieves a high AUROC of 0.6545 while requiring only 14.6s of runtime, 12.5 GFLOPS, and 97.4M parameters. This is 17 \times faster than C-Mamba for a minimal drop in AUROC. These results underscore that SimBaMM offers strong per-

formance without the substantial computational overhead associated with other methods, positioning it as a practical and effective solution. A parameter-matched analysis was not performed since it is non-trivial to determine how to equitably allocate a fixed parameter budget, e.g., whether to up- or downscale the encoders, the fusion module, or the classifier head. More details in Section C.

4.4. Case Study

To illustrate how common evaluation practices can affect reported results, we highlight methodological challenges that can compromise the validity of conclusions. The Crema-D dataset is widely used in multimodal learning, yet its official repository does not provide standardized cross-validation splits. It states only that subject-independence should be ensured when generating them, leaving this critical decision to individual researchers. We examine AUG (Jiang et al., 2025)⁵ as a representative and recent example of how these issues can affect reported results. Based on the original publication, AUG appears to outperform a broad range of multimodal learning methods with an innovative boosting algorithm, supported by ablation studies, bar charts, sensitivity analyses, and t-SNE (Maaten & Hinton, 2008) plots. However, except of tabular results, these validations are reported exclusively on Crema-D. AUG follows the splits from OGM, which uses only training and test sets, and model selection is performed on the test set. Furthermore, the splits are not subject-independent despite the dataset repository’s explicit guidance, resulting in subject leakage. Additionally, different optimizers are used across datasets, complicating fair comparisons. When we introduce a standardized dataset split protocol, generalize the implementation of AUG to M modalities, and tune hyperparameters, we observe that

⁵Published at NeurIPS 2025 with an oral presentation.

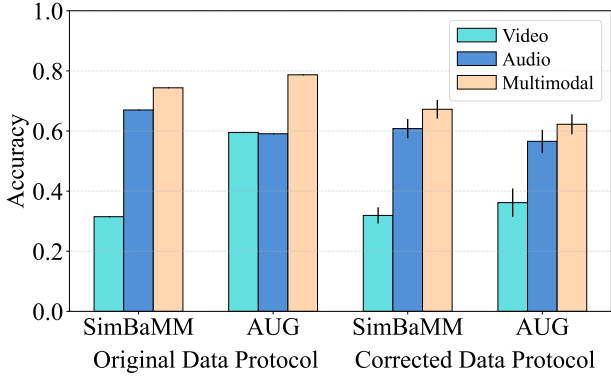


Figure 4. Case study on the CREMA-D dataset. Under a corrected data protocol with subject-independent splits and consistent hyperparameter tuning, the relative performance of methods changes.

AUG continues to boost unimodal video performance. However, it does not improve multimodal performance relative to simpler baselines. Consequently, the relative ordering shifts from AUG outperforming SimBaMM to SimBaMM matching or exceeding AUG (Figure 4). While acknowledging the theoretical contributions of AUG, this demonstrates how common evaluation practices can influence conclusions. Details in Section E.

5. Discussion

5.1. Main Drivers of Multimodal Learning

Given our empirical results that complex SOTA multimodal models do not yield reliable performance gains, a critical question arises: If methodological novelty is not the answer, what are the true drivers of multimodal performance? We argue that most problems framed as multimodal are, in fact, general machine learning challenges. Consider the core motivations behind the methods in our study: non-alignment, differential learning dynamics across modalities, dominant modality suppression, missing modality imputation, and distribution heterogeneity. These challenges arise equally in unimodal learning when combining heterogeneous feature groups, or when learning from features with varying predictive strength. The distinction between *modalities* and *feature groups within a modality* is largely semantic. If these problems do not require specific solutions in unimodal contexts, it is unclear why they would require such solutions in multimodal contexts. This suggests that the performance of any multimodal architecture is anchored to the quality of its unimodal representations. For example, in unimodal learning, the paradigm shift from Convolutional Neural Networks (CNNs) (LeCun et al., 2015) to ViTs (Dosovitskiy et al., 2021) improved visual feature extraction. A multimodal model using a ViT backbone benefits from this, even before any fusion is applied. Similarly, innovations in attention, e.g., local, global, or windowed attention, are de-

veloped in unimodal contexts (e.g., the Global Context ViT (Hatamizadeh et al., 2023)) before possibly being adapted to multimodal architectures. The gains from these components are substantial, yet they are not multimodal innovations. The true performance drivers may be the underlying unimodal parts, while the specific choice of a more complex multimodal method may offer only marginal, if any, benefit.

5.2. Reliability Checklist for Multimodal Learning

To ensure comparable and trustworthy results in future work, we recommend the following pragmatic best practices:

(1) Standardize experimental conditions: Use the same optimizers, weight initialization, data splits, and training protocols across all methods. **(2) Use identical base architectures:** When claiming benefit from a specific contribution, use an identical base architecture for both the proposed method and baselines. **(3) Include baselines:** Include simple and unimodal baselines such as SimBaMM to verify that observed gains stem from the proposed contribution rather than confounding factors. **(4) Tune all methods rigorously:** Perform hyperparameter tuning for both the proposed method and baselines. **(5) Use proper cross-validation and reporting:** Employ cross-validation with subject-independent splits and report mean \pm SD rather than single-run results. **(6) Evaluate across multiple diverse datasets:** Assess generalizability by testing methods across multiple diverse and preferably large datasets.

6. Conclusion & Future Work

We challenged the pursuit of architectural novelty in multimodal learning with a large-scale empirical study reimplementing 19 SOTA models across nine diverse datasets. Our analysis reveals that complex methods were at best practically equivalent to our proposed SimBaMM, with none showing strong evidence of meaningful performance gains. Our findings motivate a shift in emphasis: from architectural novelty alone to rigorous evaluation that verifies generalizable improvements. In many settings we study, careful tuning and strong baselines explain most of the observed gains. We demonstrate that performance is more robustly driven by rigorous hyperparameter tuning, sound methodological evaluation, and strong unimodal encoders, rather than by multimodal architectural novelty. Future work could include a similar analysis of other model families, such as early-fusion and MoE architectures, as well as methods employing other training strategies like pre-training, contrastive learning, or meta-learning. Another objective could be to develop a unified, all-inclusive model based on SimBaMM.

Acknowledgements We would like to thank Georg v. Arnim for the support with preprocessing the INSPECT dataset. Further, we would like to thank Stefan Hegselmann, Tom Burgert, Leon Sixt and Jake Graving for their valuable feedback and discussions on this paper. The authors acknowledge the Scientific Computing of the IT Division at the Charité - Universitätsmedizin Berlin for providing computational resources that have contributed to the research results reported in this paper. This research has been conducted using the UK Biobank Resource under application number 49966. B.W. and R.E. acknowledge support by the Collaborative Research Center (SFB 1470) funded by the German Research Council (DFG).

Broader Impact and Ethics This paper presents work whose goal is to advance the field of machine learning. There are many potential societal consequences of our work, none of which we feel must be specifically highlighted here.

References

Arnab, A., Dehghani, M., Heigold, G., Sun, C., Lucic, M., and Schmid, C. Vivit: A video vision transformer. In *2021 IEEE/CVF International Conference on Computer Vision, ICCV 2021, Montreal, QC, Canada, October 10-17, 2021*, pp. 6816–6826. IEEE, 2021. doi: 10.1109/ICCV48922.2021.00676.

Baevski, A., Zhou, Y., Mohamed, A., and Auli, M. wav2vec 2.0: A framework for self-supervised learning of speech representations. In Larochelle, H., Ranzato, M., Hadsell, R., Balcan, M.-F., and Lin, H.-T. (eds.), *Advances in Neural Information Processing Systems 33: Annual Conference on Neural Information Processing Systems 2020, NeurIPS 2020, December 6-12, 2020, virtual*, 2020.

Bastico, M., Ryckelynck, D., Corté, L., Tillier, Y., and Decencière, E. A simple and robust framework for cross-modality medical image segmentation applied to vision transformers. In *IEEE/CVF International Conference on Computer Vision, ICCV 2023 - Workshops, Paris, France, October 2-6, 2023*, pp. 4130–4140. IEEE, 2023. doi: 10.1109/ICCVW60793.2023.00446.

Benavoli, A., Corani, G., Demšar, J., and Zaffalon, M. Time for a change: a tutorial for comparing multiple classifiers through bayesian analysis. *Journal of Machine Learning Research*, 18(77):1–36, 2017.

Buzzega, P., Boschini, M., Porrello, A., Abati, D., and CALDERARA, S. Dark experience for general continual learning: a strong, simple baseline. In Larochelle, H., Ranzato, M., Hadsell, R., Balcan, M. F., and Lin, H. (eds.), *Advances in Neural Information Processing Systems*, volume 33, pp. 15920–15930. Curran Associates, Inc., 2020.

Cao, B., Xia, Y., Ding, Y., Zhang, C., and Hu, Q. Predictive dynamic fusion. In Salakhutdinov, R., Kolter, Z., Heller, K., Weller, A., Oliver, N., Scarlett, J., and Berkenkamp, F. (eds.), *Proceedings of the 41st International Conference on Machine Learning*, volume 235 of *Proceedings of Machine Learning Research*, pp. 5608–5628. PMLR, July 2024.

Cao, H., Cooper, D. G., Keutmann, M. K., Gur, R. C., Nenkova, A., and Verma, R. Crema-d: Crowd-sourced emotional multimodal actors dataset. *IEEE Trans. Affect. Comput.*, 5(4):377–390, 2014. doi: 10.1109/TAFFC.2014.2336244.

Caranzano, I., Pancotti, C., Rollo, C., Sartori, F., Liò, P., Fariselli, P., and Sanavia, T. Sparsity is all you need: Rethinking biological pathway-informed approaches in deep learning. arXiv:2505.04300 [q-bio], May 2025.

Chan, T.-H., Jia, K., Gao, S., Lu, J., Zeng, Z., and Ma, Y. Pcanet: A simple deep learning baseline for image classification? *IEEE Transactions on Image Processing*, 24(12):5017–5032, December 2015. ISSN 1057-7149, 1941-0042. doi: 10.1109/TIP.2015.2475625. arXiv:1404.3606 [cs].

Chen, H., Luong, V., Mukherjee, L., and Singh, V. Simpletm: A simple baseline for multivariate time series forecasting. In *Proceedings of the 13th International Conference on Learning Representations*, Singapore, 2025.

Chen, Y., Wei, F., Sun, X., Wu, Z., and Lin, S. A simple multi-modality transfer learning baseline for sign language translation. In *IEEE/CVF Conference on Computer Vision and Pattern Recognition, CVPR 2022, New Orleans, LA, USA, June 18-24, 2022*, pp. 5110–5120. IEEE, 2022. doi: 10.1109/CVPR52688.2022.00506.

Corani, G., Benavoli, A., Demšar, J., Mangili, F., and Zaffalon, M. Statistical comparison of classifiers through bayesian hierarchical modelling. *Machine Learning*, 106: 1817–1837, 2017.

Defazio, A., Yang, X., Khaled, A., Mishchenko, K., Mehta, H., and Cutkosky, A. The road less scheduled. In Globersons, A., Mackey, L., Belgrave, D., Fan, A., Paquet, U., Tomczak, J. M., and Zhang, C. (eds.), *Advances in Neural Information Processing Systems 38: Annual Conference on Neural Information Processing Systems 2024, NeurIPS 2024, Vancouver, BC, Canada, December 10 - 15, 2024*, 2024.

Devlin, J., Chang, M.-W., Lee, K., and Toutanova, K. Bert: Pre-training of deep bidirectional transformers for language understanding. In Burstein, J., Doran, C., and Solorio, T. (eds.), *Proceedings of the 2019 Conference of*

the North American Chapter of the Association for Computational Linguistics: Human Language Technologies, NAACL-HLT 2019, Minneapolis, MN, USA, June 2-7, 2019, Volume 1 (Long and Short Papers), pp. 4171–4186. Association for Computational Linguistics, 2019. doi: 10.18653/V1/N19-1423.

Dong, H., Nejjar, I., Sun, H., Chatzi, E., and Fink, O. Simmdg: A simple and effective framework for multi-modal domain generalization. In *Advances in Neural Information Processing Systems (NeurIPS)*, 2023.

Dosovitskiy, A., Beyer, L., Kolesnikov, A., Weissenborn, D., Zhai, X., Unterthiner, T., Dehghani, M., Minderer, M., Heigold, G., Gelly, S., Uszkoreit, J., and Houlsby, N. An image is worth 16x16 words: Transformers for image recognition at scale. In *9th International Conference on Learning Representations, ICLR 2021, Virtual Event, Austria, May 3-7, 2021*. OpenReview.net, 2021.

Falcon, W. and The PyTorch Lightning team. PyTorch Lightning, March 2019.

Ghahremani, M. and Wachinger, C. Regbn: Batch normalization of multimodal data with regularization. In Oh, A., Naumann, T., Globerson, A., Saenko, K., Hardt, M., and Levine, S. (eds.), *Advances in Neural Information Processing Systems 36: Annual Conference on Neural Information Processing Systems 2023, NeurIPS 2023, New Orleans, LA, USA, December 10 - 16, 2023*, 2023.

Godbole, V., Dahl, G. E., Gilmer, J., Shallue, C. J., and Nado, Z. Deep learning tuning playbook, 2023. Version 1.0.

Goyal, A., Law, H., Liu, B., Newell, A., and Deng, J. Revisiting point cloud shape classification with a simple and effective baseline. In Meila, M. and Zhang, T. (eds.), *Proceedings of the 38th International Conference on Machine Learning, ICML 2021, 18-24 July 2021, Virtual Event*, volume 139 of *Proceedings of Machine Learning Research*, pp. 3809–3820. PMLR, 2021.

Hatamizadeh, A., Yin, H., Heinrich, G., Kautz, J., and Molchanov, P. Global context vision transformers. In Krause, A., Brunskill, E., Cho, K., Engelhardt, B., Sabato, S., and Scarlett, J. (eds.), *International Conference on Machine Learning, ICML 2023, 23-29 July 2023, Honolulu, Hawaii, USA*, volume 202 of *Proceedings of Machine Learning Research*, pp. 12633–12646. PMLR, 2023.

He, H., Ye, M., Zhang, J., Liu, J., Du, B., and Tao, D. Gomatching: A simple baseline for video text spotting via long and short term matching. In Globersons, A., Mackey, L., Belgrave, D., Fan, A., Paquet, U., Tomczak, J. M., and Zhang, C. (eds.), *Advances in Neural Information Processing Systems 38: Annual Conference on Neural Information Processing Systems 2024, NeurIPS 2024, Vancouver, BC, Canada, December 10 - 15, 2024*, 2024.

He, K., Zhang, X., Ren, S., and Sun, J. Deep residual learning for image recognition. In *2016 IEEE Conference on Computer Vision and Pattern Recognition, CVPR 2016, Las Vegas, NV, USA, June 27-30, 2016*, pp. 770–778. IEEE Computer Society, 2016. doi: 10.1109/CVPR.2016.90.

Hegselmann, S., Arnim, G. v., Rheude, T., Kronenberg, N., Sontag, D., Hindricks, G., Eils, R., and Wild, B. Large language models are powerful electronic health record encoders. arXiv:2502.17403 [cs], October 2025.

Heil, B. J., Hoffman, M. M., Markowetz, F., Lee, S.-I., Greene, C. S., and Hicks, S. C. Reproducibility standards for machine learning in the life sciences. *Nature Methods*, 18(10):1132–1135, October 2021. ISSN 1548-7091, 1548-7105. doi: 10.1038/s41592-021-01256-7.

Huang, S.-C., Huo, Z., Steinberg, E., Chiang, C.-C., Lungen, M. P., Langlotz, C., Yeung, S., Shah, N., and Fries, J. A. Inspect: A multimodal dataset for pulmonary embolism diagnosis and prognosis. In *Thirty-seventh Conference on Neural Information Processing Systems Datasets and Benchmarks Track*, 2023.

Huang, X., Wu, J., Liu, H., Tang, X., and Zhou, Y. Medvthinker: Simple baselines for multimodal medical reasoning. arXiv:2508.02669 [cs], August 2025.

Jiang, Q.-Y., Huang, L., and Yang, Y. Rethinking multimodal learning from the perspective of mitigating classification ability disproportion. In *The Thirty-ninth Annual Conference on Neural Information Processing Systems*, 2025.

Kapoor, S. and Narayanan, A. Leakage and the reproducibility crisis in machine-learning-based science. *Patterns*, 4(9):100804, September 2023. ISSN 26663899. doi: 10.1016/j.patter.2023.100804.

Kirsch, A., Farquhar, S., Atighehchian, P., Jesson, A., Branchaud-Charron, F., and Gal, Y. Stochastic batch acquisition: A simple baseline for deep active learning. *Transactions on Machine Learning Research*, 2023, 2023. ISSN 2835-8856.

LeCun, Y., Bengio, Y., and Hinton, G. Deep learning. *Nature*, 521(7553):436–444, May 2015. ISSN 0028-0836, 1476-4687. doi: 10.1038/nature14539.

Li, D., Shi, X., Zhang, Y., Cheung, K. C., See, S., Wang, X., Qin, H., and Li, H. A simple baseline for video restoration with grouped spatial-temporal shift. In *IEEE/CVF Conference on Computer Vision and Pattern Recognition, CVPR 2023, Vancouver, BC, Canada, June 17-24, 2023*, 2023.

pp. 9822–9832. IEEE, 2023a. doi: 10.1109/CVPR52729. 2023.00947.

Li, J., Selvaraju, R. R., Gotmare, A., Joty, S. R., Xiong, C., and Hoi, S. C.-H. Align before fuse: Vision and language representation learning with momentum distillation. In Ranzato, M., Beygelzimer, A., Dauphin, Y. N., Liang, P., and Vaughan, J. W. (eds.), *Advances in Neural Information Processing Systems 34: Annual Conference on Neural Information Processing Systems 2021, NeurIPS 2021, December 6-14, 2021, virtual*, pp. 9694–9705, 2021.

Li, J., Ohanyan, M., Goel, V., Navasardyan, S., Wei, Y., and Shi, H. Videomatt: A simple baseline for accessible real-time video matting. In *Proceedings of the IEEE/CVF Conference on Computer Vision and Pattern Recognition (CVPR) Workshops*, pp. 2177–2186, June 2023b.

Li, S., Chen, C., and Han, J. Simmlm: A simple framework for multi-modal learning with missing modality. *CoRR*, abs/2507.19264, 2025. doi: 10.48550/ARXIV.2507.19264. arXiv: 2507.19264.

Li, W., Zhou, H., Yu, J., Song, Z., and Yang, W. Coupled mamba: Enhanced multimodal fusion with coupled state space model. In Globerson, A., Mackey, L., Belgrave, D., Fan, A., Paquet, U., Tomczak, J., and Zhang, C. (eds.), *Advances in Neural Information Processing Systems*, volume 37, pp. 59808–59832. Curran Associates, Inc., 2024.

Liang, P. P., Lim, Y. C., Tsai, Y.-H. H., Salakhutdinov, R., and Morency, L.-P. Strong and simple baselines for multimodal utterance embeddings. In *North American Chapter of the Association for Computational Linguistics*, 2019.

Liang, P. P., Lyu, Y., Fan, X., Wu, Z., Cheng, Y., Wu, J., Chen, L. Y., Wu, P., Lee, M. A., Zhu, Y., et al. Multibench: Multiscale benchmarks for multimodal representation learning. In *Thirty-fifth Conference on Neural Information Processing Systems Datasets and Benchmarks Track (Round 1)*, 2021.

Lin, L., Fan, H., Zhang, Z., Xu, Y., and Ling, H. Swintrack: A simple and strong baseline for transformer tracking. In Koyejo, S., Mohamed, S., Agarwal, A., Belgrave, D., Cho, K., and Oh, A. (eds.), *Advances in Neural Information Processing Systems 35: Annual Conference on Neural Information Processing Systems 2022, NeurIPS 2022, New Orleans, LA, USA, November 28 - December 9, 2022*, 2022.

Lipton, Z. C. and Steinhardt, J. Research for practice: troubling trends in machine-learning scholarship. *Communications of the ACM*, 62(6):45–53, May 2019. ISSN 0001-0782, 1557-7317. doi: 10.1145/3316774.

Liu, Y., Yuan, Z., Mao, H., Liang, Z., Yang, W., Qiu, Y., Cheng, T., Li, X., Xu, H., and Gao, K. Make acoustic and visual cues matter: Ch-sims v2.0 dataset and avmixup consistent module. In Tumuluri, R., Sebe, N., Pingali, G., Jayagopi, D. B., Dhall, A., Singh, R., Anthony, L., and Salah, A. A. (eds.), *International Conference on Multimodal Interaction, ICMI 2022, Bengaluru, India, November 7-11, 2022*, pp. 247–258. ACM, 2022a. doi: 10.1145/3536221.3556630.

Liu, Z., Shen, Y., Lakshminarasimhan, V. B., Liang, P. P., Zadeh, A., and Morency, L.-P. Efficient low-rank multimodal fusion with modality-specific factors. In Gurevych, I. and Miyao, Y. (eds.), *Proceedings of the 56th Annual Meeting of the Association for Computational Linguistics, ACL 2018, Melbourne, Australia, July 15-20, 2018, Volume 1: Long Papers*, pp. 2247–2256. Association for Computational Linguistics, 2018. doi: 10.18653/V1/P18-1209.

Liu, Z., Mao, H., Wu, C.-Y., Feichtenhofer, C., Darrell, T., and Xie, S. A convnet for the 2020s. In *IEEE/CVF Conference on Computer Vision and Pattern Recognition, CVPR 2022, New Orleans, LA, USA, June 18-24, 2022*, pp. 11966–11976. IEEE, 2022b. doi: 10.1109/CVPR52688.2022.01167.

Liu, Z., Liu, Q., Chen, J., Huang, S., and Luo, W. simplekt: A simple but tough-to-beat baseline for knowledge tracing. In *The Eleventh International Conference on Learning Representations, ICLR 2023, Kigali, Rwanda, May 1-5, 2023*. OpenReview.net, 2023.

Ma, M., Ren, J., Zhao, L., Tulyakov, S., Wu, C., and Peng, X. Smil: Multimodal learning with severely missing modality. In *Thirty-Fifth AAAI Conference on Artificial Intelligence, AAAI 2021, Thirty-Third Conference on Innovative Applications of Artificial Intelligence, IAAI 2021, The Eleventh Symposium on Educational Advances in Artificial Intelligence, EAAI 2021, Virtual Event, February 2-9, 2021*, pp. 2302–2310. AAAI Press, 2021. doi: 10.1609/AAAI.V35I3.16330.

Ma, M., Ren, J., Zhao, L., Testuggine, D., and Peng, X. Are multimodal transformers robust to missing modality? In *IEEE/CVF Conference on Computer Vision and Pattern Recognition, CVPR 2022, New Orleans, LA, USA, June 18-24, 2022*, pp. 18156–18165. IEEE, 2022. doi: 10.1109/CVPR52688.2022.01764.

Maaten, L. v. d. and Hinton, G. Visualizing data using t-sne. *Journal of Machine Learning Research*, 9(86): 2579–2605, 2008.

Maddox, W. J., Izmailov, P., Garipov, T., Vetrov, D. P., and Wilson, A. G. A simple baseline for bayesian uncertainty in deep learning. In Wallach, H. M., Larochelle, H.,

Beygelzimer, A., d’Alché Buc, F., Fox, E. B., and Garnett, R. (eds.), *Advances in Neural Information Processing Systems 32: Annual Conference on Neural Information Processing Systems 2019, NeurIPS 2019, December 8-14, 2019, Vancouver, BC, Canada*, pp. 13132–13143, 2019.

Manolache, A.-M., Tantaru, D.-C., and Nieuport, M. Molmix: A simple yet effective baseline for multimodal molecular representation learning. In *Advances in Neural Information Processing Systems 38: Annual Conference on Neural Information Processing Systems 2024, Machine Learning in Structural Biology Workshop, NeurIPS 2024, Vancouver, BC, Canada, December 10 - 15, 2024*, 2024.

McDermott, M. The (lack of?) science of machine learning for healthcare. In Hegselmann, S., Zhou, H., Healey, E., Chang, T., Ellington, C., Mhasawade, V., Tonekaboni, S., Argaw, P., and Zhang, H. (eds.), *Proceedings of the 4th Machine Learning for Health Symposium*, volume 259 of *Proceedings of Machine Learning Research*, pp. 19–29. PMLR, December 2025.

Memmel, M., Bachmann, R., and Zamir, A. Modality-invariant visual odometry for embodied vision. In *Proceedings of the IEEE/CVF Conference on Computer Vision and Pattern Recognition*, pp. 21549–21559, 2023.

Nagrani, A., Yang, S., Arnab, A., Jansen, A., Schmid, C., and Sun, C. Attention bottlenecks for multimodal fusion. In Ranzato, M., Beygelzimer, A., Dauphin, Y. N., Liang, P., and Vaughan, J. W. (eds.), *Advances in Neural Information Processing Systems 34: Annual Conference on Neural Information Processing Systems 2021, NeurIPS 2021, December 6-14, 2021, virtual*, pp. 14200–14213, 2021.

Nezakati, N., Reza, M. K., Patil, A., Solh, M., and Asif, M. S. Mmp: Towards robust multi-modal learning with masked modality projection. arXiv:2410.03010 [cs], October 2024.

Peebles, W. and Xie, S. Scalable diffusion models with transformers. In *IEEE/CVF International Conference on Computer Vision, ICCV 2023, Paris, France, October 1-6, 2023*, pp. 4172–4182. IEEE, 2023. doi: 10.1109/ICCV51070.2023.00387.

Peng, X., Wei, Y., Deng, A., Wang, D., and Hu, D. Balanced multimodal learning via on-the-fly gradient modulation. In *IEEE/CVF Conference on Computer Vision and Pattern Recognition, CVPR 2022, New Orleans, LA, USA, June 18-24, 2022*, pp. 8228–8237. IEEE, 2022. doi: 10.1109/CVPR52688.2022.00806.

Pineau, J., Vincent-Lamarre, P., Sinha, K., Lariviere, V., Beygelzimer, A., d’Alché Buc, F., Fox, E., and Larochelle, H. Improving reproducibility in machine learning research(a report from the neurips 2019 reproducibility program). *Journal of Machine Learning Research*, 22(164):1–20, 2021.

Prabhu, A., Torr, P. H. S., and Dokania, P. K. Gdumb: A simple approach that questions our progress in continual learning. In Vedaldi, A., Bischof, H., Brox, T., and Frahm, J.-M. (eds.), *Computer Vision - ECCV 2020 - 16th European Conference, Glasgow, UK, August 23-28, 2020, Proceedings, Part II*, volume 12347 of *Lecture Notes in Computer Science*, pp. 524–540. Springer, 2020. doi: 10.1007/978-3-030-58536-5_31.

Press, O., Schneider, S., Kümmerer, M., and Bethge, M. Rdumb: A simple approach that questions our progress in continual test-time adaptation. In Oh, A., Naumann, T., Globerson, A., Saenko, K., Hardt, M., and Levine, S. (eds.), *Advances in Neural Information Processing Systems 36: Annual Conference on Neural Information Processing Systems 2023, NeurIPS 2023, New Orleans, LA, USA, December 10 - 16, 2023*, 2023.

Rheude, T., Eils, R., and Wild, B. Cohort-based active modality acquisition. arXiv:2505.16791 [cs], December 2025.

Saporta, A., Puli, A., Goldstein, M., and Ranganath, R. Contrasting with symile: Simple model-agnostic representation learning for unlimited modalities. In *Advances in Neural Information Processing Systems*, 2024.

Semmelrock, H., Ross-Hellauer, T., Kopeinik, S., Theiler, D., Haberl, A., Thalmann, S., and Kowald, D. Reproducibility in machine-learning-based research: Overview, barriers, and drivers. *AI Mag.*, 46(2), 2025. doi: 10.1002/AAAI.70002.

Shi, J., Zhong, Y., Xu, N., Li, Y., and Xu, C. A simple baseline for weakly-supervised scene graph generation. In *2021 IEEE/CVF International Conference on Computer Vision, ICCV 2021, Montreal, QC, Canada, October 10-17, 2021*, pp. 16373–16382. IEEE, 2021. doi: 10.1109/ICCV48922.2021.01608.

Shukor, M., Fini, E., Costa, V. G. T. d., Cord, M., Susskind, J., and El-Nouby, A. Scaling laws for native multimodal models scaling laws for native multimodal models. arXiv:2504.07951 [cs], April 2025.

Soenksen, L. R., Ma, Y., Zeng, C., Boussioux, L., Vilalobos Carballo, K., Na, L., Wiberg, H. M., Li, M. L., Fuentes, I., and Bertsimas, D. Integrated multimodal artificial intelligence framework for healthcare applications. *npj Digital Medicine*, 5(1):149, September 2022a. ISSN 2398-6352. doi: 10.1038/s41746-022-00689-4.

Soenksen, L. R., Ma, Y., Zeng, C., Boussioux, L. D. J., Vilalobos Carballo, K., Na, L., Wiberg, H., Li, M., Fuentes, I., and Bertsimas, D. Code for generating the haim multimodal dataset of mimic-iv clinical data and x-rays, 2022b.

Song, A. H., Chen, R. J., Jaume, G., Vaidya, A. J., Baras, A., and Mahmood, F. Multimodal prototyping for cancer survival prediction. In Salakhutdinov, R., Kolter, Z., Heller, K., Weller, A., Oliver, N., Scarlett, J., and Berkenkamp, F. (eds.), *Proceedings of the 41st International Conference on Machine Learning*, volume 235 of *Proceedings of Machine Learning Research*, pp. 46050–46073. PMLR, July 2024.

Steinberg, E., Fries, J. A., Xu, Y., and Shah, N. Motor: A time-to-event foundation model for structured medical records. In *The Twelfth International Conference on Learning Representations*, 2024.

Sudlow, C., Gallacher, J., Allen, N., Beral, V., Burton, P., Danesh, J., Downey, P., Elliott, P., Green, J., Landray, M., Liu, B., Matthews, P., Ong, G., Pell, J., Silman, A., Young, A., Sprosen, T., Peakman, T., and Collins, R. Uk biobank: An open access resource for identifying the causes of a wide range of complex diseases of middle and old age. *PLOS Medicine*, 12(3):e1001779, March 2015. ISSN 1549-1676. doi: 10.1371/journal.pmed.1001779.

Tsai, Y.-H. H., Bai, S., Liang, P. P., Kolter, J. Z., Morency, L.-P., and Salakhutdinov, R. Multimodal transformer for unaligned multimodal language sequences. In Korhonen, A., Traum, D. R., and Márquez, L. (eds.), *Proceedings of the 57th Conference of the Association for Computational Linguistics, ACL 2019, Florence, Italy, July 28-August 2, 2019, Volume 1: Long Papers*, pp. 6558–6569. Association for Computational Linguistics, 2019. doi: 10.18653/V1/P19-1656.

Vaswani, A., Shazeer, N., Parmar, N., Uszkoreit, J., Jones, L., Gomez, A. N., Kaiser, L., and Polosukhin, I. Attention is all you need. In Guyon, I., Luxburg, U. v., Bengio, S., Wallach, H. M., Fergus, R., Vishwanathan, S. V. N., and Garnett, R. (eds.), *Advances in Neural Information Processing Systems 30: Annual Conference on Neural Information Processing Systems 2017, December 4-9, 2017, Long Beach, CA, USA*, pp. 5998–6008, 2017.

Vishniakov, K., Viswanathan, K., Medvedev, A., Kanithi, P. K., Pimentel, M. A., Rajan, R., and Khan, S. Genomic foundationless models: Pretraining does not promise performance. placeholder, December 2024.

Wang, H., Chen, Y., Ma, C., Avery, J., Hull, L., and Carneiro, G. Multi-modal learning with missing modality via shared-specific feature modelling. In *IEEE/CVF Conference on Computer Vision and Pattern Recognition, CVPR 2023, Vancouver, BC, Canada, June 17-24, 2023*, pp. 15878–15887. IEEE, 2023a. doi: 10.1109/CVPR52729.2023.01524.

Wang, W., Tran, D., and Feiszli, M. What makes training multi-modal classification networks hard? In *2020 IEEE/CVF Conference on Computer Vision and Pattern Recognition, CVPR 2020, Seattle, WA, USA, June 13-19, 2020*, pp. 12692–12702. Computer Vision Foundation / IEEE, 2020. doi: 10.1109/CVPR42600.2020.01271.

Wang, Y., Li, Y., and Cui, Z. Incomplete multimodality-diffused emotion recognition. In Oh, A., Naumann, T., Globerson, A., Saenko, K., Hardt, M., and Levine, S. (eds.), *Advances in Neural Information Processing Systems 36: Annual Conference on Neural Information Processing Systems 2023, NeurIPS 2023, New Orleans, LA, USA, December 10 - 16, 2023*, 2023b.

Wei, S., Luo, C., and Luo, Y. Boosting multimodal learning via disentangled gradient learning. In *2025 IEEE/CVF International Conference on Computer Vision, ICCV 2025, Honolulu, Hawaii, October 19-23, 2025*. IEEE, 2025a.

Wei, S., Luo, C., and Luo, Y. Improving multimodal learning via imbalanced learning. In *2025 IEEE/CVF International Conference on Computer Vision, ICCV 2025, Honolulu, Hawaii, October 19-23, 2025*. IEEE, 2025b.

Wei, Y. and Hu, D. Mmpareto: Boosting multimodal learning with innocent unimodal assistance. In Salakhutdinov, R., Kolter, Z., Heller, K., Weller, A., Oliver, N., Scarlett, J., and Berkenkamp, F. (eds.), *Proceedings of the 41st International Conference on Machine Learning*, volume 235 of *Proceedings of Machine Learning Research*, pp. 52559–52572. PMLR, July 2024.

Wu, N., Jastrzebski, S., Cho, K., and Geras, K. J. Characterizing and overcoming the greedy nature of learning in multi-modal deep neural networks. In Chaudhuri, K., Jegelka, S., Song, L., Szepesvari, C., Niu, G., and Sabato, S. (eds.), *Proceedings of the 39th International Conference on Machine Learning*, volume 162 of *Proceedings of Machine Learning Research*, pp. 24043–24055. PMLR, July 2022.

Wu, Q., Shao, Y., Wang, J., and Sun, X. Learning optimal multimodal information bottleneck representations. In *Forty-second International Conference on Machine Learning*, 2025.

Wu, R., Wang, H., Chen, H.-T., and Carneiro, G. Deep multimodal learning with missing modality: A survey. arXiv:2409.07825 [cs], October 2024.

Xia, Y., Yang, X., Liu, Z., Liu, Z., Song, L., and Bian, J. Position: Rethinking post-hoc search-based neural approaches for solving large-scale traveling salesman

problems. In *Forty-first International Conference on Machine Learning, ICML 2024, Vienna, Austria, July 21-27, 2024*. OpenReview.net, 2024.

Xin, Y., Ates, G. C., Gong, K., and Shao, W. Med3dvlm: An efficient vision-language model for 3d medical image analysis. arXiv: 2503.20047, 2025.

Xu, W., Liu, Y., He, L., Huang, X., and Jiang, L. Xmodel-vlm: A simple baseline for multimodal vision language model. arXiv:2405.09215 [cs], June 2024.

Yu, W., Xu, H., Meng, F., Zhu, Y., Ma, Y., Wu, J., Zou, J., and Yang, K. Ch-sims: A chinese multimodal sentiment analysis dataset with fine-grained annotation of modality. In *Proceedings of the 58th Annual Meeting of the Association for Computational Linguistics*, pp. 3718–3727, Online, 2020. Association for Computational Linguistics. doi: 10.18653/v1/2020.acl-main.343.

Zadeh, A., Zellers, R., Pincus, E., and Morency, L.-P. Mosi: Multimodal corpus of sentiment intensity and subjectivity analysis in online opinion videos. arXiv:1606.06259 [cs], August 2016.

Zadeh, A., Liang, P. P., Poria, S., Cambria, E., and Morency, L.-P. Multimodal language analysis in the wild: Cmu-mosei dataset and interpretable dynamic fusion graph. In *Annual Meeting of the Association for Computational Linguistics*, 2018.

Zhang, Y., Pfahringer, B., Frank, E., Bifet, A., Lim, N. J. S., and Jia, Y. A simple but strong baseline for online continual learning: Repeated augmented rehearsal. In Koyejo, S., Mohamed, S., Agarwal, A., Belgrave, D., Cho, K., and Oh, A. (eds.), *Advances in Neural Information Processing Systems 35: Annual Conference on Neural Information Processing Systems 2022, NeurIPS 2022, New Orleans, LA, USA, November 28 - December 9, 2022*, 2022.

Zhang, Y., Li, M., Long, D., Zhang, X., Lin, H., Yang, B., Xie, P., Yang, A., Liu, D., Lin, J., Huang, F., and Zhou, J. Qwen3 embedding: Advancing text embedding and reranking through foundation models. arXiv:2506.05176 [cs], June 2025.

Zhao, H., Andriushchenko, M., Croce, F., and Flammarion, N. Long is more for alignment: A simple but tough-to-beat baseline for instruction fine-tuning. In Salakhutdinov, R., Kolter, Z., Heller, K., Weller, A., Oliver, N., Scarlett, J., and Berkenkamp, F. (eds.), *Proceedings of the 41st International Conference on Machine Learning*, volume 235 of *Proceedings of Machine Learning Research*, pp. 60674–60703. PMLR, July 2024.

Zhou, Z., Zhou, S., Lv, Z., Zou, M., Tang, Y., and Liang, J. A simple baseline for efficient hand mesh reconstruction. In *Proceedings of the IEEE/CVF Conference on Computer Vision and Pattern Recognition (CVPR)*, pp. 1367–1376, June 2024.

Zuo, R., Wei, F., Chen, Z., Mak, B., Yang, J., and Tong, X. A simple baseline for spoken language to sign language translation with 3d avatars. In Leonardis, A., Ricci, E., Roth, S., Russakovsky, O., Sattler, T., and Varol, G. (eds.), *Computer Vision - ECCV 2024 - 18th European Conference, Milan, Italy, September 29-October 4, 2024, Proceedings, Part XLIX*, volume 15107 of *Lecture Notes in Computer Science*, pp. 36–54. Springer, 2024. doi: 10.1007/978-3-031-72967-6_3.

A. Method Re-Implementation Details

For every method, weight initialization is applied throughout the entire architecture, including encoders and method-specific extensions (Kaiming initialization for linear and convolutional layers with biases set to zero, constant values for the weight (1.0) and bias (0.0) of LayerNorm layers, and Gaussian initialization for additional parameters). Model-related blocks, *e.g.*, for Transformers or ResNets, are not re-initialized specifically. For Transformer blocks, sinusoidal positional encodings are used. To improve reproducibility and ensure faithful re-implementations, we contacted the first and last author of all benchmarked methods by sharing our preprint and code repository, inviting them to review the corresponding re-implementation details and report any discrepancies.

A.1. Data

For **IMDer**, we followed the official code repository for our re-implementation but modernized the original implementation to align with SimBaMM (Rheude et al., 2025). While IMDer proposed a U-Net style score network, our implementation leverages a more modern Diffusion Transformer (DiT) (Peebles & Xie, 2023) backbone, which has shown superior performance. Unlike the original work, we do not pre-train on all modalities before evaluating with missing modalities. For **MMP** and **ShaSpec**, we followed the official code repository for our re-implementation.

A.2. Encoder

For **RegBN**, we followed the official code repository for our re-implementation but corrected a deviation in which the secondary modality features (g) were incorrectly used to optimize the Tikhonov regularizer (λ). Our implementation uses the primary modality features (f) as required by the paper’s equations (Eq. 4 and 11), ensuring the regularization correctly models the relationship between the modalities. To handle the nested gradient computations of the internal L-BFGS optimization, we isolate this sub-problem by detaching its input tensors from the main computation graph. For **AUG**, we followed the official code repository for our re-implementation. In addition to changes for scaling the method to M modalities, we implement the classifier as a Transformer (with pre-norm to ensure stability) for fair efficiency comparisons with other methods.

A.3. Fusion

For **PDF**, we followed the official code repository for our re-implementation. We define the ground-truth confidence p_{true} as the sample-wise average of the predicted probabilities for the correct binary outcomes across all labels. Furthermore, we extend the concept of distribution uniformity for

relative calibration to the Binary Cross Entropy (BCE) context by calculating it as the average deviation from 0.5 (the point of maximum uncertainty). This allows the full PDF mechanism, including both the co-belief calculation and relative calibration, to function effectively for multi-class and multi-label problems alike. For **Coupled Mamba**, as no official code was available, we implemented the method from scratch following the paper. Our re-implementation mirrors the paper’s design, structured into Coupled Mamba Blocks and Coupled Mamba Layers. To handle real-world data imperfections, our implementation robustly manages both variable sequence lengths through dynamic padding and masked pooling. The central coupled scan is implemented as a sequential operation to precisely match the paper’s recurrence relation. Unfortunately, given time constraints and the absence of it from the official repository, the global kernel for optimization efficiency could not be implemented. For **OMIB**, as no official code was available, we implemented the method from scratch following the paper. The modality fusion, *i.e.*, the Cross-Attention Network, is implemented as a multi-layer Transformer encoder, while the probabilistic mapping in the OMF block is handled by standard Variational Auto Encoders (VAEs) with linear heads. The model supports both fixed-size and variable-length sequence inputs, unifying the processing logic internally and ensuring alignment with the paper’s two-phase training and dynamic regularization principles. For **MBT** and **LMF**, we followed the official code repository for our re-implementation.

A.4. Head

For **MuLT**, we followed the official code repository for our re-implementation except for using post-norm instead of pre-norm for consistency with the other implemented methods.

A.5. Gradient

For **OGM** and **OGM-GE**, we followed the official code repository for our re-implementation. A linear layer must be used instead of a Transformer for the fusion of the encoder’s embeddings. The method relies on a simple linear layer where the weights corresponding to each modality can be isolated. This is not possible with a Transformer, as self-attention creates a non-linear dependency on all inputs. For **BMML**, we followed the official code repository for our re-implementation, but we designated the shared fusion Transformer as the bypass branch and the individual unimodal encoders as the main branches. For **G-Blend**, there is no official code repository published, so we implemented the method from scratch following the paper. For **DGL**, **ARL**, and **MMPareto**, we followed the official code repository for our re-implementation.

Table 5. Tabular representation of the efficiency of the methods w.r.t. the number of parameters, training time, and FLOPS.

Group	Method	#Parameters (M) ↓	FLOPs (G) ↓	Training Time (sec/epoch) ↓
Data	IMDer (Wang et al., 2023b)	103.0	408.23	203.50
	MMP (Nezakati et al., 2024)	98.1	12.57	15.42
	ShaSpec (Wang et al., 2023a)	103.0	11.14	17.45
Encoder	RegBN (Ghahremani & Wachinger, 2023)	97.4	11.15	43.21
	AUG (Jiang et al., 2025)	97.4	11.10	12.15
Fusion	MBT (Nagrani et al., 2021)	99.4	11.11	18.62
	LMF (Liu et al., 2018)	97.9	11.09	11.83
	PDF (Cao et al., 2024)	95.9	11.08	11.94
	Coupled Mamba (Li et al., 2024)	94.9	10.63	253.80
	OMIB (Wu et al., 2025)	98.3	11.11	12.34
Head	MulT (Tsai et al., 2019)	113.0	15.32	18.20
Gradient	OGM (Peng et al., 2022)	95.8	11.08	11.13
	OGM ^{GE} (Peng et al., 2022)	95.8	11.08	12.27
	DGL (Wei et al., 2025a)	97.4	11.14	13.20
	ARL (Wei et al., 2025b)	97.4	11.10	12.52
	MMPareto (Wei & Hu, 2024)	97.4	11.10	11.78
	BMML (Wu et al., 2022)	97.4	11.10	11.47
	G-Blend ^{Online} (Wang et al., 2020)	97.4	11.10	11.98
	G-Blend ^{Offline} (Wang et al., 2020)	97.4	11.10	11.85
	SimBaMM ^{CLS}	97.3	11.10	11.74
	SimBaMM	97.4	12.46	14.58

B. Compute Environment

Our experiments are conducted on a High-Performance Cluster (HPC) with the following environment:

- 21 Dell PowerEdge R7525 compute nodes, each with 64 AMD Epyc cores (Rome), 512GB RAM and 1 NVIDIA A100 40G GPU
- 2 Dell PowerEdge XE8545 compute nodes, each with 128 AMD Epyc cores (Milan), 512GB RAM, 4 NVIDIA A100 40G GPUs (NVLink-connected)

All efficiency-related experiments are done on the first, *i.e.*, single-GPU compute node.

C. Detailed Efficiency Analysis

In addition to the tables representing efficiency vs. performance, Figure 5 and Table 5 present a focused view on efficiency comparisons.

D. Dataset Details

MIMIC Symile The MIMIC Symile dataset provides a challenging clinical benchmark for multi-label diagnostic prediction. Derived from the MIMIC database, it comprises 10 345 samples collected from patients in intensive care units. The task is to predict the presence of ten conditions: Fracture, Enlarged Cardiomediastinum, Consolidation,

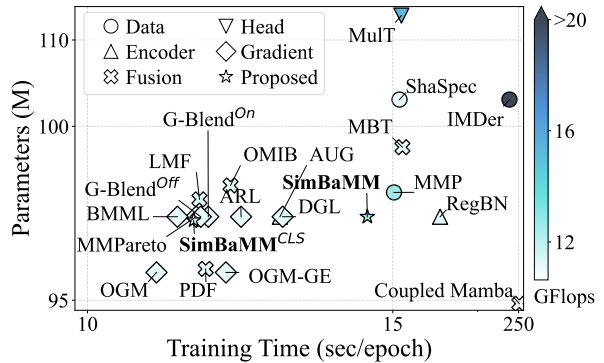


Figure 5. Visual representation of the efficiency of the methods w.r.t. the number of parameters, training time, and FLOPS.

tion, Atelectasis, Edema, Cardiomegaly, Lung Lesion, Lung Opacity, Pneumonia, and Pneumothorax. Our evaluation leverages three distinct data types: laboratory test results, chest X-ray images, and electrocardiograms (ECGs). We use an MLP for laboratory tests, a ViT for vision data, and a Transformer encoder for ECGs. The ECG samples are preprocessed by removing baseline wander.

MIMIC HAIM Similarly, the MIMIC HAIM dataset is a healthcare benchmark focused on the same ten-class diagnostic prediction task as Symile. This bimodal dataset is substantially larger, containing 45 050 samples. For this dataset, our experiments utilize laboratory values and chest

X-ray images as the two input modalities. We use an MLP for laboratory tests and a ViT for vision data.

INSPECT The INSPECT dataset (Huang et al., 2023) comprises 22 449 CT pulmonary angiography (CTPA) studies for pulmonary embolism (PE) diagnosis, combining 3D computer-assisted tomography (CT) images with longitudinal electronic health records (EHRs). We focus on the binary PE detection task, where approximately 20% of cases are PE-positive. We use MOTOR (Steinberg et al., 2024) embeddings for structured EHR data and Med3dVLM (Xin et al., 2025) embeddings (latest vision encoder stage with global average pooling on the feature maps) for the CT volumes, in combination with MLP encoders.

Table 6. Unimodal performance of the modalities for the healthcare datasets. For the UKB, if unimodal data is not available for a sample, it is zero-imputed to ensure a fair comparison to the multimodal performance.

Modality	AUROC \uparrow
<i>HAIM</i>	
X-ray	0.7042 \pm 0.020
Laboratory	0.6654 \pm 0.038
<i>Symile</i>	
X-ray	0.6453 \pm 0.030
Laboratory	0.5597 \pm 0.010
ECG	0.4960 \pm 0.024
<i>INSPECT</i>	
CT	0.5825 \pm 0.007
EHR	0.6568 \pm 0.003
<i>UKB</i>	
Metabolomics	0.7108 \pm 0.003
EHR	0.7560 \pm 0.010
Proteomics	0.5434 \pm 0.009
Polygenic risk score (PRS)	0.6008 \pm 0.008
Blood biochemistry	0.7156 \pm 0.004
Baseline characteristics	0.7151 \pm 0.004
Local environment	0.5049 \pm 0.009
Arterial stiffness	0.5290 \pm 0.016
Anthropometry	0.6086 \pm 0.025
Blood pressure	0.6403 \pm 0.008
ECG	0.5298 \pm 0.017
Eye measures	0.5233 \pm 0.014
Bone densitometry	0.5853 \pm 0.003
Grip strength	0.5227 \pm 0.008
Spirometry	0.6668 \pm 0.021
Touchscreen	0.7334 \pm 0.007
Cognitive function	0.5956 \pm 0.006
Hearing	0.5355 \pm 0.020
Interview	0.6803 \pm 0.005
Blood count	0.6810 \pm 0.005
Urine assays	0.5384 \pm 0.006
Telomeres	0.5670 \pm 0.010
Infectious diseases	0.5008 \pm 0.001

UKB The UKB is a large, long-term prospective biobank study with 488 131 samples after preprocessing and exclu-

sions. While various targets, *e.g.*, for survival analysis are possible, we chose to predict ten-year mortality from the recruitment date for simplicity. It comprises 23 modalities, *i.e.*, metabolomics, EHR, PRS, proteomics, blood biochemistry, environment, stiffness, anthropometry, blood pressure, ECG, eye measures, bone densitometry, grip strength, spirometry, touchscreen, cognitive function, hearing tests, interviews, blood counts, urine assays, telomeres, and infectious diseases. The UKB category IDs used for the structured field extraction are: 220 (NMR metabolomics), 1838 (Proteomics), 100008 (Anthropometry), 100007 (Arterial stiffness), 100094 (Baseline characteristics), 17518 (Blood biochemistry), 100081 (Blood count), 100011 (Blood pressure), 100018 (Bone densitometry of heel), 100026 (Cognitive function), 104 (ECG at rest), 100012 (ECG during exercise), 100013 (Eye measures), 300/264/100313 (Genetics), 100019 (Hand grip strength), 100049 (Hearing test), 51428 (Infectious diseases), 113 (Local environment), 100020 (Spirometry), 265 (Telomeres), 100025 (Touchscreen), 100083 (Urine assays), and 100071 (Verbal interview). We use MLPs for all modalities and raw inputs except for the EHR modality, for which we use QWEN (Zhang et al., 2025) embeddings based on previously used serializations (Hegselmann et al., 2025). Individual missing entries within a modality were imputed with zeros, and instances where a feature vector was entirely absent were excluded.

Table 7. Unimodal performance of the modalities for the UKB without zero imputation, *i.e.*, only the available modality subset is used.

Modality	AUROC \uparrow
Metabolomics	0.7118 \pm 0.004
EHR	0.7728 \pm 0.005
Proteomics	0.7588 \pm 0.018
PRS	0.6009 \pm 0.009
Blood biochemistry	0.7183 \pm 0.004
Baseline characteristics	0.7150 \pm 0.006
Local environment	0.5025 \pm 0.004
Arterial stiffness	0.5997 \pm 0.009
Anthropometry	0.6060 \pm 0.013
Blood pressure	0.6388 \pm 0.009
ECG	0.6869 \pm 0.005
Eye measures	0.5669 \pm 0.045
Bone densitometry	0.6008 \pm 0.002
Grip strength	0.5212 \pm 0.008
Spirometry	0.6615 \pm 0.004
Touchscreen	0.7180 \pm 0.006
Cognitive function	0.5956 \pm 0.005
Hearing	0.6020 \pm 0.009
Interview	0.6656 \pm 0.006
Blood count	0.6838 \pm 0.006
Urine assays	0.5284 \pm 0.009
Telomeres	0.5685 \pm 0.009
Infectious diseases	0.5330 \pm 0.027

CMU-MOSI and CMU-MOSEI Shifting from the clinical domain, the CMU-MOS(E)I dataset is a benchmark for multimodal sentiment analysis and emotion recognition. It consists of 2199 (MOSI) and 22 856 (MOSEI) video clips of speakers expressing opinions, with annotations for seven emotional classes. The data is trimodal, encompassing visual, acoustic, and linguistic information. A key distinction from the other datasets is the use of the officially provided pre-computed feature embeddings, in contrast to processing raw data. We use BERT for language sequences and a Transformer encoder for the vision and audio embeddings.

CH-SIMS and CH-SIMS 2 These datasets are benchmarks for multimodal sentiment analysis and emotion recognition. They consist of 2281 (CH-SIMS) and 4403 (CH-SIMS 2) video clips of speakers expressing emotions. Similar to MOS(E)I, they are trimodal but provide raw data. We use Wav2Vec2, ViViT, and BERT for the audio, video, and language data, respectively.

Crema-D Crema-D is a dataset for multimodal sentiment analysis with six emotion classes (such as anger and fear) that can be further subdivided into a more fine-grained set of 24 classes. It consists of 7442 samples and provides audio and video data. Following related work, we use spectrograms in combination with a ResNet for the audio data and video frames in combination with another ResNet for the vision data. For the case study, we use horizontal flipping augmentations and ImageNet normalization values analogous to the AUG code repository.

E. Case Study Details

Especially for the case study, alternative viewpoints on our set of implementation choices are possible. Therefore, we record key concerns, add further experiments and explain how they relate to the case study.

On the Necessity of Reusing Splits for Fair Comparison It is often argued that new methods should use legacy data splits to ensure numbers are directly comparable to previous tables. Comparability with prior results is a pragmatic concern, but we do not consider reusing legacy splits as a methodological requirement. In particular, when existing splits are underspecified or violate stated dataset guidance, *e.g.*, subject independence, adopting a standardized, leakage-avoiding protocol is justified even if it breaks comparability with earlier reports. Rather than treating inherited splits as binding, we view them as one point in the design space: authors can report results on legacy splits for continuity while also providing results under a corrected protocol to support valid conclusions. In this sense, the case study targets evaluation practice, *i.e.*, how conclusions shift under a more defensible protocol, rather than attributing shortcomings to

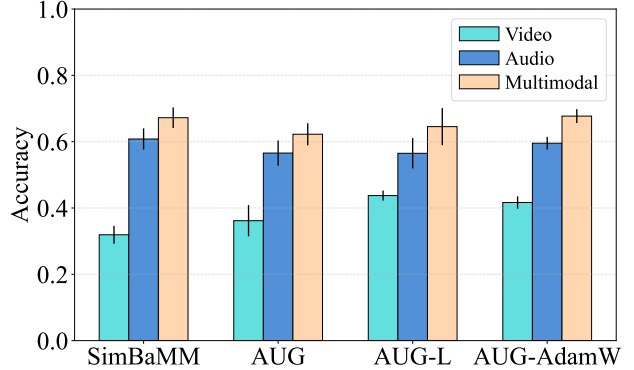


Figure 6. Alternative configurations for AUG in the case study setting with the corrected data protocol, *i.e.*, with a linear head (AUG-L) and another optimizer (AUG-AdamW).

any single method or paper.

AUG with Linear Head We replace AUG’s original linear head with a Transformer-based head to align the architectural capacity with other compared methods. To verify that this choice does not drive our conclusions, we additionally show that AUG with a linear head performs similarly (AUG-L, Figure 6). AUG shows the same overall performance trends and leads to the same conclusions about its relative behavior in the multimodal setting, indicating that the case study findings are not an artifact of the Transformer head.

Different Optimizers To assess whether our conclusions depend on the choice of optimizer, we performed an additional hyperparameter sweep using AdamW instead of the originally used SGD (AUG-AdamW, Figure 6). To circumvent learning rate schedulers, we still the use ScheduleFree variant. This change does not alter the qualitative outcome: the relative behavior of AUG and the baselines, as well as the resulting ranking trends that motivate the case study, remain consistent. This indicates that our headline conclusions are not an artifact of selecting a particular optimizer family, but persist under a substantially different optimization setup.

Sweep on Full Parameter Space One may argue that initializing AUG’s sweep from architectural choices selected for our method, *e.g.*, encoder and head dimensions, could bias the comparison, and that AUG should instead be tuned from scratch over the full design space, including architectural hyperparameters as well as optimization settings. This concern is addressed by AUG-L (Figure 6), since all model hyperparameters are swept in this setting, except of the encoders which are set to the originally used ResNet18s. The resulting performance and qualitative trends are unchanged: the relative conclusions of the case study and the observed method ranking remain consistent. This indicates that our findings are robust to the hyperparameter

search procedure and do not arise from anchoring AUG to architectural choices optimized for a different method.

F. Statistical Comparison Across Datasets

To rigorously compare methods across datasets, we employ Bayesian hierarchical analysis following Benavoli et al. (2017); Corani et al. (2017). The model uses fold-level cross-validation results, accounts for correlation between folds due to overlapping training sets, and yields direct posterior probabilities for each pairwise comparison.

F.1. Bayesian Hierarchical Pairwise Comparisons

For each pair of methods (i, j) , we compare their fold-level cross-validation results across the datasets on which both methods are available. Let $x_{d,f} = s_{d,i,f} - s_{d,j,f}$ be the per-fold performance difference on dataset d . We model within-dataset differences as correlated observations due to shared training data in K -fold cross-validation:

$$\mathbf{x}_d \sim \mathcal{N}(\mu_d \mathbf{1}, \Sigma_d), \quad \rho = 1/K, \quad (1)$$

where K is the number of folds (here $K = 5$, thus $\rho = 0.2$). Dataset-level mean differences are modeled with a robust population distribution:

$$\mu_d \sim t(\delta_0, \sigma_0, \nu), \quad (2)$$

where δ_0 is the population-level mean difference and ν represents the degrees of freedom, accounting for non-normality. We define a ROPE of $\pm\epsilon$ (here $\epsilon = 0.01$ in absolute metric points). Following Corani et al. (2017), we report the posterior probabilities that each of three outcomes is the *most probable* outcome on a new dataset drawn from the population distribution $\delta_{\text{new}} \sim t(\delta_0, \sigma_0, \nu)$: *method j better* ($\delta_{\text{new}} < -\epsilon$), *practically equivalent* ($|\delta_{\text{new}}| \leq \epsilon$), and *method i better* ($\delta_{\text{new}} > \epsilon$). Concretely, for each posterior draw of $(\delta_0, \sigma_0, \nu)$ we compute the three region probabilities for δ_{new} and count which region has the largest probability; the reported values are the resulting frequencies. We complete the model with the following hyperpriors based on the robust ranges identified in Corani et al. (2017):

$$\delta_0 \sim \mathcal{U}(-1, 1), \quad (3)$$

$$\sigma_0 \sim \mathcal{U}(0, \bar{s}_0), \quad (4)$$

$$\nu \sim \text{Gamma}(\alpha, \beta) + 1, \quad (5)$$

$$\alpha \sim \mathcal{U}(1.0, 2.0), \quad \beta \sim \mathcal{U}(0.01, 0.10). \quad (6)$$

Following Corani et al. (2017), we set $\bar{s}_0 = 1000 s_{\bar{x}}$, where $s_{\bar{x}}$ is the standard deviation across datasets of the per-dataset mean differences $\bar{x}_d = \frac{1}{K} \sum_{f=1}^K x_{d,f}$.

Reported quantities For every comparison, we additionally report the posterior mean and 95% credible interval of the population-level mean difference δ_0 (absolute metric points; $\delta_0 > 0$ indicates method i is better on average).

Table 8. Comparison with the best unimodal baseline.

Method	P(base >other)	P(\approx)	P(other >base)	$\mathbb{E}[\delta_0]$	95% CI
CoupledMamba	0.18	0.10	0.72	-0.010	[-0.038, 0.024]
SimBaMM-CLS	0.41	0.06	0.53	-0.002	[-0.031, 0.031]
MMPareto	0.66	0.08	0.26	0.013	[-0.026, 0.066]
ARL	0.19	0.14	0.67	-0.008	[-0.034, 0.024]
GBlend-On	0.61	0.10	0.29	0.011	[-0.029, 0.062]
BMML	0.59	0.03	0.38	0.006	[-0.035, 0.056]
OGM-GE	0.80	0.02	0.18	0.017	[-0.024, 0.060]
MulT	0.29	0.67	0.04	0.006	[-0.008, 0.025]
SimBaMM-Full	0.74	0.14	0.13	0.021	[-0.023, 0.083]
MBT	0.91	0.03	0.06	0.021	[-0.009, 0.054]
GBlend-Off	0.73	0.18	0.08	0.015	[-0.014, 0.046]
LMF	0.93	0.00	0.07	0.057	[-0.020, 0.142]
OMIB	0.96	0.00	0.04	0.033	[-0.007, 0.075]
OGM	0.80	0.05	0.14	0.018	[-0.020, 0.064]
PDF	0.95	0.03	0.03	0.023	[-0.002, 0.050]
AUG	0.94	0.02	0.04	0.031	[-0.005, 0.072]
RegBN	0.68	0.04	0.27	0.013	[-0.026, 0.067]
DGL	0.98	0.00	0.02	0.083	[0.009, 0.161]

Handling missingness Missing method-dataset pairs are handled via pairwise complete cases: for a comparison (i, j) we include only datasets where *both* methods have fold-level results available.

Model fitting and diagnostics We fit the model with NUTS using PyMC (nutpie backend) with four chains (2000 warmup and 4000 post-warmup draws per chain). We monitor \hat{R} , effective sample size (ESS), divergences, and max tree depth hits for the key parameters $(\delta_0, \sigma_0, \nu)$ to ensure reliable posterior estimates. When diagnostics are poor, we automatically re-sample with a more conservative target acceptance rate and/or a larger draw budget. Table 14 summarizes these diagnostics for the baseline comparisons reported in Tables 4 and 8.

Bounded-metric sanity check Since the evaluated metrics are bounded in $[0, 1]$, the dataset-level mean difference satisfies $\delta \in [-1, 1]$. We therefore compute a simple posterior predictive check: the probability that a new dataset-level effect drawn from the fitted population distribution violates this bound, i.e., $P(|\delta_{\text{new}}| > 1)$. For the baseline comparisons in Table 14, this probability is negligible, indicating the fitted population model places essentially no mass outside the feasible range.

F.2. ROPE Sensitivity

To assess how sensitive our conclusions are to the practical significance threshold, we repeat the comparisons with $\epsilon \in \{0.005, 0.01, 0.02\}$ (i.e., ROPE $\pm 0.5\%$, $\pm 1\%$, and $\pm 2\%$ in absolute metric points). Tables 4 and 8 correspond to $\epsilon = 0.01$; additional ROPE settings are reported below.

Key takeaway The qualitative conclusions reported in Section 4.2 are robust to reasonable ROPE choices: tightening the ROPE makes more comparisons count as “wins” by a small margin (reducing $P(\approx)$), whereas widening the ROPE shifts probability toward practical equivalence. Importantly, the posterior on δ_0 (mean and 95% credible interval) is unchanged; only the partitioning into *win* / *ROPE* / *loss* depends on ϵ .

Comparison to SimBaMM^{CLS} For the strongest competitors, the interpretation changes smoothly with ϵ . For example, CoupledMamba has $P(\text{CoupledMamba} > \text{SimBaMM-CLS}) = 0.64$ under $\epsilon = 0.005$ (Table 9), but this drops to 0.30 under $\epsilon = 0.01$ (Table 4) and to 0.04 under $\epsilon = 0.02$ (Table 10), while $P(\approx)$ increases from $0.28 \rightarrow 0.67 \rightarrow 0.95$. Thus, if a $\geq 1\%$ improvement is considered practically meaningful (as in Section 4.2), no method shows strong evidence of outperforming SimBaMM-CLS; if a tighter threshold is used, CoupledMamba appears more likely to be *slightly* better, consistent with a small estimated mean effect (Table 4 reports $\mathbb{E}[\delta_0] \approx -0.006$ for SimBaMM-CLS minus CoupledMamba).

Comparison to the best unimodal baseline The sensitivity analysis suggests that improvements over the best unimodal baseline (when present) are typically modest: CoupledMamba and ARL are likely to beat the unimodal baseline for $\epsilon \in \{0.005, 0.01\}$ (e.g., $P(\text{CoupledMamba} > \text{Unimodal}) = 0.79/0.72$ and $P(\text{ARL} > \text{Unimodal}) = 0.76/0.67$ for $\epsilon = 0.005/0.01$), but these probabilities decrease to 0.37 and 0.28 at $\epsilon = 0.02$ with $P(\approx)$ becoming dominant (Table 12). This supports the interpretation in Section 4.2 that any gains over unimodal baselines are not reliably large in absolute terms.

F.3. ρ and Prior-Bound Sensitivity

We follow the correlation heuristic $\rho = 1/K$ and the weakly-informative uniform scale priors recommended by Corani et al. (2017). To ensure conclusions are not driven by these modeling choices, we additionally repeat the baseline comparisons using (i) an alternative fold-correlation heuristic $\rho = 1/(K-1)$ and (ii) tighter upper bounds for the uniform scale priors. Table 13 reports the maximum absolute changes in the reported probabilities and $\mathbb{E}[\delta_0]$ under these perturbations.

Sensitivity result The sensitivity results show that conclusions are stable: across the baseline comparisons, the win/ROPE/loss probabilities change by at most 0.053 and the population-level mean effect estimates $\mathbb{E}[\delta_0]$ shift by at most 0.002 under these alternative settings (Table 13).

Table 9. Comparison with SimBaMM-CLS (ROPE $\pm 0.5\%$).

Method	$P(\text{base} > \text{other})$	$P(\approx)$	$P(\text{other} > \text{base})$	$\mathbb{E}[\delta_0]$	95% CI
CoupledMamba	0.07	0.28	0.64	-0.006	[-0.021, 0.006]
Best unimodal	0.56	0.00	0.44	0.002	[-0.031, 0.031]
MMPareto	0.23	0.32	0.45	-0.002	[-0.019, 0.022]
ARL	0.45	0.18	0.37	0.002	[-0.019, 0.028]
GBlend-On	0.48	0.23	0.29	0.005	[-0.018, 0.045]
BMML	0.79	0.00	0.21	0.013	[-0.021, 0.051]
OGM-GE	0.89	0.03	0.08	0.015	[-0.009, 0.042]
MuLT	0.47	0.13	0.41	0.002	[-0.023, 0.031]
SimBaMM-Full	0.62	0.07	0.31	0.007	[-0.038, 0.056]
MBT	0.90	0.05	0.05	0.012	[-0.004, 0.028]
GBlend-Off	0.95	0.01	0.05	0.021	[-0.005, 0.048]
LMF	0.90	0.00	0.10	0.049	[-0.028, 0.142]
OMIB	0.98	0.00	0.02	0.022	[0.003, 0.043]
OGM	0.95	0.01	0.04	0.017	[-0.003, 0.040]
PDF	0.99	0.00	0.01	0.020	[0.005, 0.037]
AUG	0.97	0.00	0.03	0.032	[-0.000, 0.066]
RegBN	0.92	0.03	0.05	0.014	[-0.004, 0.039]
DGL	0.98	0.00	0.02	0.078	[0.006, 0.158]

Sampler diagnostics We summarize standard MCMC diagnostics for the baseline comparisons (Table 14): the maximum split- \hat{R} across the key parameters (δ_0, σ_0, ν), the minimum bulk and tail effective sample sizes (ESS), and whether any fits exhibit NUTS divergences or max-treedepth hits. We also report the maximum posterior predictive probability $P(|\delta_{\text{new}}| > 1)$ as a bounded-metric sanity check.

Diagnostics result The sampler diagnostics indicate adequate convergence and effective sampling for the baseline comparisons: split- \hat{R} is close to 1 (max 1.01), ESS values are above common thresholds (min bulk/tail ESS 439/108), and we observe no divergences or max-treedepth issues (Table 14).

G. Hyperparameter Search

We use Bayesian optimization minimizing the validation loss without sweeping the batch size (Godbole et al., 2023). In the following, we list the hyperparameter search space and configurations structured by the dataset and the evaluated methods. The former refers to the encoders used, while the latter refers primarily to the remaining groups. The initial SimBaMM is swept with 500 runs while the other methods are swept with an additional 100 runs.

G.1. Encoders Parameter Space

The parameter spaces for the individual datasets are shown in Listings 1 to 9.

Table 10. Comparison with SimBaMM-CLS (ROPE $\pm 2\%$).

Method	P(base >other)	P(\approx)	P(other >base)	$E[\delta_0]$	95% CI
CoupledMamba	0.01	0.95	0.04	-0.006	[-0.021,0.006]
Best unimodal	0.25	0.53	0.22	0.002	[-0.031,0.031]
MMPareto	0.05	0.91	0.04	-0.002	[-0.019,0.022]
ARL	0.11	0.84	0.06	0.002	[-0.019,0.028]
GBlend-On	0.21	0.74	0.05	0.005	[-0.018,0.045]
BMML	0.51	0.38	0.11	0.013	[-0.021,0.051]
OGM-GE	0.38	0.59	0.03	0.015	[-0.009,0.042]
MuLT	0.13	0.79	0.08	0.002	[-0.023,0.031]
SimBaMM-Full	0.30	0.57	0.14	0.007	[-0.038,0.056]
MBT	0.14	0.85	0.01	0.012	[-0.004,0.028]
GBlend-Off	0.61	0.38	0.01	0.021	[-0.005,0.048]
LMF	0.87	0.04	0.10	0.049	[-0.028,0.142]
OMIB	0.65	0.35	0.01	0.022	[0.003,0.043]
OGM	0.37	0.62	0.01	0.017	[-0.003,0.040]
PDF	0.46	0.54	0.00	0.020	[0.005,0.037]
AUG	0.88	0.11	0.02	0.032	[-0.000,0.066]
RegBN	0.29	0.71	0.01	0.014	[-0.004,0.039]
DGL	0.98	0.00	0.02	0.078	[0.006,0.158]

```

1 # Encoders
2 vision.vit.vit:
3   values: ["vit_b_16", "vit_b_32"]
4 vision.vit.dropout:
5   values: [0, 0.1, 0.2]
6 sequential.transformer.num_hidden_layers:
7   values: [2, 4, 6, 8]
8 sequential.transformer.num_attention_heads:
9   values: [2, 4, 8, 16]
10 sequential.transformer.intermediate_size:
11   values: [256, 512, 1024, 2048]
12 sequential.transformer.dropout:
13   values: [0, 0.1, 0.2]

```

Listing 1. Hyperparameter search space configuration for MIMIC HAIM.

G.2. Methods Parameter Space

The parameter spaces for the individual methods are shown in Listings 10 to 27.

 Table 11. Comparison with the best unimodal baseline (ROPE $\pm 0.5\%$).

Method	P(base >other)	P(\approx)	P(other >base)	$E[\delta_0]$	95% CI
CoupledMamba	0.20	0.02	0.79	-0.010	[-0.038,0.024]
SimBaMM-CLS	0.44	0.00	0.56	-0.002	[-0.031,0.031]
MMPareto	0.69	0.02	0.29	0.013	[-0.026,0.066]
ARL	0.23	0.02	0.76	-0.008	[-0.034,0.024]
GBlend-On	0.65	0.02	0.33	0.011	[-0.029,0.062]
BMML	0.60	0.00	0.40	0.006	[-0.035,0.056]
OGM-GE	0.81	0.00	0.19	0.017	[-0.024,0.060]
MuLT	0.63	0.28	0.09	0.006	[-0.008,0.025]
SimBaMM-Full	0.80	0.04	0.16	0.021	[-0.023,0.083]
MBT	0.94	0.00	0.06	0.021	[-0.009,0.054]
GBlend-Off	0.84	0.04	0.12	0.015	[-0.014,0.046]
LMF	0.93	0.00	0.07	0.057	[-0.020,0.142]
OMIB	0.96	0.00	0.04	0.033	[-0.007,0.075]
OGM	0.84	0.01	0.16	0.018	[-0.020,0.064]
PDF	0.97	0.00	0.03	0.023	[-0.002,0.050]
AUG	0.95	0.01	0.04	0.031	[-0.005,0.072]
RegBN	0.71	0.00	0.29	0.013	[-0.026,0.067]
DGL	0.98	0.00	0.02	0.083	[0.009,0.161]

```

1 # Encoders
2 vision.vit.vit:
3   values: ["vit_b_16", "vit_b_32"]
4 vision.vit.dropout:
5   values: [0, 0.1, 0.2]
6 sequential1.transformer.num_hidden_layers:
7   values: [2, 4, 6, 8]
8 sequential1.transformer.num_attention_heads:
9   values: [2, 4, 8, 16]
10 sequential1.transformer.intermediate_size:
11   values: [256, 512, 1024, 2048]
12 sequential1.transformer.dropout:
13   values: [0, 0.1, 0.2]
14 sequential2.mlp.hidden_dims:
15   values: [[256, 512, 256], [512, 1024, 512], [1024, 2048, 1024]]
16 sequential2.mlp.hidden_dropouts:
17   values: [[0.0, 0.0, 0.0], [0.1, 0.1, 0.1], [0.2, 0.2, 0.2]]
18
19

```

Listing 2. Hyperparameter search space configuration for MIMIC Symile.

```

1 # Encoders
2 vision.mlp.hidden_dims:
3   values: [[1024, 512, 256], [512, 256, 128], [256, 128, 64], [128, 64, 32]]
4 vision.mlp.hidden_dropouts:
5   values: [[0.0, 0.0, 0.0], [0.1, 0.1, 0.1], [0.2, 0.2, 0.2]]
6 ehr.mlp.hidden_dims:
7   values: [[1024, 512, 256], [512, 256, 128], [256, 128, 64], [128, 64, 32]]
8 ehr.mlp.hidden_dropouts:
9   values: [[0.0, 0.0, 0.0], [0.1, 0.1, 0.1], [0.2, 0.2, 0.2]]
10
11
12
13

```

Listing 3. Hyperparameter search space configuration for IN-SPECT.

Table 12. Comparison with the best unimodal baseline (ROPE $\pm 2\%$).

Method	P(base >other)	P(\approx >base)	P(other >base)	$\mathbb{E}[\delta_0]$	95% CI
CoupledMamba	0.10	0.52	0.37	-0.010	[-0.038, 0.024]
SimBaMM-CLS	0.22	0.53	0.25	-0.002	[-0.031, 0.031]
MM Pareto	0.52	0.34	0.14	0.013	[-0.026, 0.066]
ARL	0.09	0.63	0.28	-0.008	[-0.034, 0.024]
GBlend-On	0.46	0.38	0.16	0.011	[-0.029, 0.062]
BMMIL	0.43	0.34	0.23	0.006	[-0.035, 0.056]
OGM-GE	0.66	0.22	0.12	0.017	[-0.024, 0.060]
MuLT	0.07	0.92	0.01	0.006	[-0.008, 0.025]
SimBaMM-Full	0.54	0.39	0.07	0.021	[-0.023, 0.083]
MBT	0.61	0.36	0.03	0.021	[-0.009, 0.054]
GBlend-Off	0.40	0.56	0.03	0.015	[-0.014, 0.046]
LMF	0.93	0.01	0.07	0.057	[-0.020, 0.142]
OMIB	0.90	0.06	0.04	0.033	[-0.007, 0.075]
OGM	0.58	0.33	0.08	0.018	[-0.020, 0.064]
PDF	0.68	0.31	0.01	0.023	[-0.002, 0.050]
AUG	0.83	0.15	0.02	0.031	[-0.005, 0.072]
RegBN	0.51	0.35	0.15	0.013	[-0.026, 0.067]
DGL	0.98	0.00	0.02	0.083	[0.009, 0.161]

Table 13. Sensitivity of baseline comparisons to ρ and prior bounds.

Baseline	Metric	$\rho = 1/(K - 1)$	$\bar{s} \times 100$
SimBaMM-CLS	max $ \Delta P $ (win)	0.034	0.015
	max $ \Delta P $ (\approx)	0.053	0.024
	max $ \Delta P $ (loss)	0.024	0.024
	max $ \Delta \mathbb{E}[\delta_0] $	0.001	0.001
Best unimodal	max $ \Delta P $ (win)	0.036	0.012
	max $ \Delta P $ (\approx)	0.035	0.008
	max $ \Delta P $ (loss)	0.023	0.010
	max $ \Delta \mathbb{E}[\delta_0] $	0.002	0.001

Table 14. Sampler diagnostics for baseline comparisons.

Baseline	max \hat{R}	min ESS (bulk/tail)	div /td	max $P(\delta_{\text{new}} > 1)$
SimBaMM-CLS	1.010	439/108	0/0	7.07e-04
Best unimodal	1.010	501/320	0/0	3.86e-04

```

1 # Encoders, for all 23 modalities, exemplary:
2 nmr.mlp.hidden_dims:
3   values: [[1024, 512, 256], [512, 256, 128],
4   [256, 128, 64], [128, 64, 32]]
5 nmr.mlp.hidden_dropouts:
6   values: [[0.0, 0.0, 0.0], [0.2, 0.2, 0.2],
7   [0.3, 0.3, 0.3], [0.4, 0.4, 0.4],
8   [0.5, 0.5, 0.5], [0.6, 0.6, 0.6],
9   [0.7, 0.7, 0.7]]

```

Listing 4. Hyperparameter search space configuration for the UKB.

```

1 # Encoders
2 audio.transformer.num_hidden_layers:
3   values: [1, 4, 8, 16]
4 audio.transformer.num_attention_heads:
5   values: [1, 2, 4, 8]
6 audio.transformer.intermediate_size:
7   values: [256, 512, 1024]
8 audio.transformer.dropout:
9   values: [0.0, 0.1]
10 vision.transformer.num_hidden_layers:
11   values: [1, 4, 8, 16]
12 vision.transformer.num_attention_heads:
13   values: [1, 2, 4, 8]
14 vision.transformer.intermediate_size:
15   values: [256, 512, 1024]
16 vision.transformer.dropout:
17   values: [0.0, 0.1]

```

Listing 5. Hyperparameter search space configuration for MOSI.

```

1 # Encoders
2 audio.transformer.num_hidden_layers:
3   values: [1, 4, 8, 16]
4 audio.transformer.num_attention_heads:
5   values: [1, 2, 4, 8]
6 audio.transformer.intermediate_size:
7   values: [256, 512, 1024]
8 audio.transformer.dropout:
9   values: [0.0, 0.1]
10 vision.transformer.num_hidden_layers:
11   values: [1, 4, 8, 16]
12 vision.transformer.num_attention_heads:
13   values: [1, 2, 4, 8]
14 vision.transformer.intermediate_size:
15   values: [256, 512, 1024]
16 vision.transformer.dropout:
17   values: [0.0, 0.1]

```

Listing 6. Hyperparameter search space configuration for MOSEI.

```

1 # Encoders
2 audio.transformer.num_hidden_layers:
3   values: [1, 4, 8, 16]
4 audio.transformer.num_attention_heads:
5   values: [1, 2, 4, 8]
6 audio.transformer.intermediate_size:
7   values: [256, 512, 1024]
8 vision.transformer.num_hidden_layers:
9   values: [1, 4, 8, 16]
10 vision.transformer.num_attention_heads:
11   values: [1, 2, 4, 8]
12 vision.transformer.intermediate_size:
13   values: [256, 512, 1024]

```

Listing 7. Hyperparameter search space configuration for CHSIMS.

```

1 # Encoders
2 audio.transformer.num_hidden_layers:
3   values: [1, 4, 8, 16]
4 audio.transformer.num_attention_heads:
5   values: [1, 2, 4, 8]
6 audio.transformer.intermediate_size:
7   values: [256, 512, 1024]
8 vision.transformer.num_hidden_layers:
9   values: [1, 4, 8, 16]
10 vision.transformer.num_attention_heads:
11   values: [1, 2, 4, 8]
12 vision.transformer.intermediate_size:
13   values: [256, 512, 1024]

```

Listing 8. Hyperparameter search space configuration for CHSIMS2.

```

1 # Encoders
2 # Standard PyTorch ResNet18s

```

Listing 9. Hyperparameter search space configuration for CREMA-D.

```

1 # Head
2 head_transformer.d_model:
3   values: [32, 64, 128, 256, 512]
4 head_transformer.dim_feedforward:
5   values: [256, 512, 1024, 2048]
6 head_transformer.dropout:
7   values: [0, 0.1, 0.2]
8 head_transformer.nhead:
9   values: [4, 8, 16]
10 head_transformer.num_layers:
11   values: [2, 4, 6, 8]
12 # Optimizer
13 optimizer.lr:
14   min: 0.000001
15   max: 0.1
16   distribution: "log_uniform_values"
17 optimizer.warmup_steps:
18   values: [0, 100, 200, 500, 1000]
19 optimizer.weight_decay:
20   values: [0, 0.1, 0.01, 0.001]

```

Listing 10. Hyperparameter search space configuration for Sim-BaMM.

```

1 # Optimizer
2 optimizer.lr:
3   min: 0.000001
4   max: 0.1
5   distribution: "log_uniform_values"
6 optimizer.warmup_steps:
7   values: [0, 100, 200, 500, 1000]
8 optimizer.weight_decay:
9   values: [0, 0.1, 0.01, 0.001]
10 # IMDer
11 imder.beta:
12   min: 0.01
13   max: 1.0
14   distribution: "log_uniform_values"
15 ddpmns.n_steps:
16   values: [10, 20, 30, 40, 50, 100]
17 ddpmns.d_model: # fixed w.r.t. Transformer d_model
18   value: 256
19 ddpmns.hidden_dim:
20   values: [32, 64, 128, 256, 512, 1024]
21 ddpmns.num_layers:
22   values: [1, 2, 3, 4, 5, 6, 7, 8]
23 ddpmns.dropout:
24   values: [0.0, 0.1, 0.2]
25 ddpmns.nhead:
26   values: [1, 2, 4, 8, 16, 32]

```

Listing 11. Hyperparameter search space configuration for IMDer.

```

1 # Optimizer
2 optimizer.lr:
3   min: 0.000001
4   max: 0.1
5   distribution: "log_uniform_values"
6 optimizer.warmup_steps:
7   values: [0, 100, 200, 500, 1000]
8 optimizer.weight_decay:
9   values: [0, 0.1, 0.01, 0.001]
10 # MMP
11 mmp.proj_mlp.hidden_dim:
12   values: [128, 256, 512, 1024]
13 mmp.proj_mlp.dropout:
14   values: [0.0, 0.1, 0.2]
15 mmp.attn_steps.dropout:
16   values: [0.0, 0.1, 0.2]
17 mmp.attn_steps.nhead:
18   values: [1, 2, 4, 8, 16]
19 mmp.num_aggregated_tokens:
20   values: [2, 4, 8, 16, 32]
21 mmp.loss_alignment_alpha:
22   min: 0.001
23   max: 1.0
24   distribution: "log_uniform_values"

```

Listing 12. Hyperparameter search space configuration for MMP.

```

1 # Optimizer
2 optimizer.lr:
3   min: 0.000001
4   max: 0.1
5   distribution: "log_uniform_values"
6 optimizer.warmup_steps:
7   values: [0, 100, 200, 500, 1000]
8 optimizer.weight_decay:
9   values: [0, 0.1, 0.01, 0.001]
10 # ShaSpec
11 shaspec.loss_alpha:
12   min: 0.01
13   max: 1.0
14   distribution: "log_uniform_values"
15 shaspec.loss_beta:
16   min: 0.001
17   max: 0.1
18   distribution: "log_uniform_values"

```

Listing 13. Hyperparameter search space configuration for ShaSpec.

```

1 # Optimizer
2 optimizer.lr:
3   min: 0.000001
4   max: 0.1
5   distribution: "log_uniform_values"
6 optimizer.warmup_steps:
7   values: [0, 100, 200, 500, 1000]
8 optimizer.weight_decay:
9   values: [0, 0.1, 0.01, 0.001]
10 # RegBN
11 rbn.reference_modality_idx: # 0-(M-1)
12   values: [0, 1, 2]
13 rbn.momentum:
14   values: [0.1, 0.01, 0.05]
15 rbn.sigma_THR:
16   values: [0.1, 0.3, 0.5]
17 rbn.sigma_MIN:
18   values: [0.01, 0.1, 0.2]
19 rbn.affine:
20   values: [True, False]

```

Listing 14. Hyperparameter search space configuration for RegBN.

```

1 # Optimizer
2 optimizer.lr:
3     min: 0.000001
4     max: 0.1
5     distribution: "log_uniform_values"
6 optimizer.warmup_steps:
7     values: [0, 100, 200, 500, 1000]
8 optimizer.weight_decay:
9     values: [0, 0.1, 0.01, 0.001]
10 # AUG
11 aug.merge_alphas:
12     values: [[0.33, 0.33, 0.33]] # 1/M
13 aug.check_interval:
14     values: [1, 5, 10, 20]
15 aug.threshold:
16     min: 0.01
17     max: 1.0
18     distribution: "log_uniform_values"
19 aug.confidence_coeff:
20     min: 0.01
21     max: 10.0
22     distribution: "log_uniform_values"
23 aug.lambda_smooth:
24     min: 0.01
25     max: 1.0
26     distribution: "log_uniform_values"

```

Listing 15. Hyperparameter search space configuration for AUG.

```

1 # Optimizer
2 optimizer.lr:
3     min: 0.000001
4     max: 0.1
5     distribution: "log_uniform_values"
6 optimizer.warmup_steps:
7     values: [0, 100, 200, 500, 1000]
8 optimizer.weight_decay:
9     values: [0, 0.1, 0.01, 0.001]
10 # PDF
11 pdf.loss_weight:
12     min: 0.01
13     max: 1.0
14     distribution: "log_uniform_values"
15 pdf.unimodal_loss_weight:
16     min: 0.01
17     max: 1.0
18     distribution: "log_uniform_values"
19 pdf.p_head.hidden_dims:
20     values: [[128], [256], [512], [1024],
21               [128, 256], [128, 256, 512],
22               [128, 256, 512, 1024]]
23 pdf.p_head.dropout:
24     values: [0.0, 0.1, 0.2]

```

Listing 18. Hyperparameter search space configuration for PDF.

```

1 # Optimizer
2 optimizer.lr:
3     min: 0.000001
4     max: 0.1
5     distribution: "log_uniform_values"
6 optimizer.warmup_steps:
7     values: [0, 100, 200, 500, 1000]
8 optimizer.weight_decay:
9     values: [0, 0.1, 0.01, 0.001]
10 # MBT
11 bottleneck.num_bottlenecks:
12     values: [1, 2, 4, 8, 16, 32]
13 bottleneck.layers:
14     values: [1, 2, 4, 8, 16, 32]
15 bottleneck.dim_feedforward:
16     values: [128, 256, 512, 1024, 2048]
17 bottleneck.nhead:
18     values: [1, 2, 4, 8, 16, 32]
19 bottleneck.dropout:
20     values: [0.0, 0.1, 0.2, 0.3, 0.4]

```

Listing 16. Hyperparameter search space configuration for MBT.

```

1 # Optimizer
2 optimizer.lr:
3     min: 0.000001
4     max: 0.1
5     distribution: "log_uniform_values"
6 optimizer.warmup_steps:
7     values: [0, 100, 200, 500, 1000]
8 optimizer.weight_decay:
9     values: [0, 0.1, 0.01, 0.001]
10 # Coupled Mamba
11 coupled_ssm.d_model:
12     values: [32, 64, 128, 256]
13 coupled_ssm.num_layers:
14     values: [2, 3, 4, 5, 6, 7, 8]
15 coupled_ssm.d_state:
16     values: [8, 16, 32, 64, 128]
17 coupled_ssm.d_conv:
18     values: [2, 4, 8, 16]
19 coupled_ssm.expand:
20     values: [1, 2, 4, 8]

```

Listing 19. Hyperparameter search space configuration for Coupled Mamba.

Listing 17. Hyperparameter search space configuration for LMF.

```

1 # Optimizer
2 optimizer.lr:
3     min: 0.000001
4     max: 0.1
5     distribution: "log_uniform_values"
6 optimizer.warmup_steps:
7     values: [0, 100, 200, 500, 1000]
8 optimizer.weight_decay:
9     values: [0, 0.1, 0.01, 0.001]
10 # LMF
11 low_rank_matrix_fusion.rank:
12     values: [2, 10, 20, 50, 100, 200, 250]

```

```

1 # Optimizer
2 optimizer.lr:
3     min: 0.000001
4     max: 0.1
5     distribution: "log_uniform_values"
6 optimizer.warmup_steps:
7     values: [0, 100, 200, 500, 1000]
8 optimizer.weight_decay:
9     values: [0, 0.1, 0.01, 0.001]
10 # OMIB
11 omib.beta:
12     min: 0.00001
13     max: 0.1
14     distribution: "log_uniform_values"
15 omib.cross_attn_network.num_layers:
16     values: [1, 2, 4, 8, 16]
17 omib.cross_attn_network.dropout:
18     values: [0.0, 0.1, 0.2]
19 omib.cross_attn_network.num_heads:
20     values: [1, 2, 4, 8, 16]
21 omib.cross_attn_network.dim_feedforward:
22     values: [128, 256, 512, 1024]
23 omib.warmup_epochs:
24     values: [0, 1, 2, 4, 8]

```

Listing 20. Hyperparameter search space configuration for OMIB.

```

1 # Optimizer
2 optimizer.lr:
3     min: 0.000001
4     max: 0.1
5     distribution: "log_uniform_values"
6 optimizer.warmup_steps:
7     values: [0, 100, 200, 500, 1000]
8 optimizer.weight_decay:
9     values: [0, 0.1, 0.01, 0.001]
10 # Mult
11 crossmodal_transformer.d_model:
12     values: [256] # = head_transformer.d_model
13 crossmodal_transformer.num_layers:
14     values: [1, 2, 4, 8, 16]
15 crossmodal_transformer.dim_feedforward:
16     values: [128, 256, 512, 1024]
17 crossmodal_transformer.nhead:
18     values: [1, 2, 4, 8, 16]
19 crossmodal_transformer.dropout:
20     values: [0.0, 0.1, 0.2, 0.5]

```

Listing 21. Hyperparameter search space configuration for Mult.

```

1 # Optimizer
2 optimizer.lr:
3     min: 0.000001
4     max: 0.1
5     distribution: "log_uniform_values"
6 optimizer.warmup_steps:
7     values: [0, 100, 200, 500, 1000]
8 optimizer.weight_decay:
9     values: [0, 0.1, 0.01, 0.001]
10 # OGM
11 ogm.alpha:
12     min: 0.01
13     max: 1.0
14     distribution: "log_uniform_values"
15 ogm.use_ge:
16     values: [False] # True for OGM-GE

```

Listing 22. Hyperparameter search space configuration for OGM and OGM-GE.

```

1 # Optimizer
2 optimizer.lr:
3     min: 0.000001
4     max: 0.1
5     distribution: "log_uniform_values"
6 optimizer.warmup_steps:
7     values: [0, 100, 200, 500, 1000]
8 optimizer.weight_decay:
9     values: [0, 0.1, 0.01, 0.001]
10 # DGL
11 dgl.unimodal_loss_weight:
12     min: 0.001
13     max: 1.0
14     distribution: "log_uniform_values"

```

Listing 23. Hyperparameter search space configuration for DGL.

```

1 # Optimizer
2 optimizer.lr:
3     min: 0.000001
4     max: 0.1
5     distribution: "log_uniform_values"
6 optimizer.warmup_steps:
7     values: [0, 100, 200, 500, 1000]
8 optimizer.weight_decay:
9     values: [0, 0.1, 0.01, 0.001]
10 # ARL
11 arl.unimodal_loss_weight:
12     min: 0.01
13     max: 1.0
14     distribution: "log_uniform_values"
15 arl.temperature:
16     min: 0.01
17     max: 1.0
18     distribution: "log_uniform_values"

```

Listing 24. Hyperparameter search space configuration for ARL.

```

1 # Optimizer
2 optimizer.lr:
3     min: 0.000001
4     max: 0.1
5     distribution: "log_uniform_values"
6 optimizer.warmup_steps:
7     values: [0, 100, 200, 500, 1000]
8 optimizer.weight_decay:
9     values: [0, 0.1, 0.01, 0.001]
10 # MMPareto
11 mmpareto.unimodal_loss_weight:
12     min: 0.01
13     max: 1.0
14     distribution: "log_uniform_values"
15 mmpareto.gamma:
16     min: 0.01
17     max: 1.0
18     distribution: "log_uniform_values"

```

Listing 25. Hyperparameter search space configuration for MM-Pareto.

```

1 # Optimizer
2 optimizer.lr:
3     min: 0.000001
4     max: 0.1
5     distribution: "log_uniform_values"
6 optimizer.warmup_steps:
7     values: [0, 100, 200, 500, 1000]
8 optimizer.weight_decay:
9     values: [0, 0.1, 0.01, 0.001]
10 # BMML
11 bmml.unimodal_loss_weight:
12     min: 0.01
13     max: 1.0
14     distribution: "log_uniform_values"
15 bmml.alpha:
16     min: 0.001
17     max: 0.1
18     distribution: "log_uniform_values"
19 bmml.q:
20     values: [3, 5, 10]
21 bmml.bmml_momentum:
22     values: [0.9, 0.99, 0.999]
23 bmml.warmup_epochs:
24     values: [0, 1, 2, 5, 10]

```

Listing 26. Hyperparameter search space configuration for BMML.

```

1 # Optimizer
2 optimizer.lr:
3     min: 0.000001
4     max: 0.1
5     distribution: "log_uniform_values"
6 optimizer.warmup_steps:
7     values: [0, 100, 200, 500, 1000]
8 optimizer.weight_decay:
9     values: [0, 0.1, 0.01, 0.001]
10 # GBlend
11 gblend.mode:
12     values: ['offline'] # Online
13 gblend.update_freq:
14     values: [1, 5, 10]
15 gblend.lookahead_epochs:
16     values: [1, 3, 5]

```

Listing 27. Hyperparameter search space configuration for G-Blend Online/Offline.